Comprehensive Tungsten–Iodine Cluster Chemistry: Isolated Intermediates in the Solid-State Nucleation of $[W_6I_{14}]^{2-}$

John D. Franolic, Jeffrey R. Long, and R. H. Holm*

Contribution from the Department of Chemistry, Harvard University, Cambridge, Massachusetts 02138

Received April 21, 1995[⊗]

Abstract: The solid state reaction between $W(CO)_6$ and iodine provides a convenient entry to a realm of tungsten–iodine cluster chemistry inaccessible via direct reaction of the elements. A thorough examination of this reaction system has been undertaken, revealing unprecedented structural information on a nucleation process that culminates with the formation of the face-capped octahedral cluster $[W_6I_{14}]^{2-}$. Heating the reactants at 140 °C invokes the release of CO gas, whereupon nucleation proceeds to form an amorphous black mixture (Phase A) containing trinuclear $[W_3I_9]^{1-}$ clusters, whose structure consists of a metal–metal bonded W_3 triangle elaborated with six edge-bridging and three vertex-capping iodides. Insoluble W_4I_{13}, a molecular phase featuring tetrahedral $[W_4I_{11}]^{1-}$ clusters dimerized through two bridging triiodide units, crystallizes when Phase A is heated at 165 °C. Further heating Phase A to 200 °C produces an amorphous solid (Phase B) that dissolves in ethanol to afford pentanuclear $[W_5I_{13}]^{1-}$ clusters, with a square-pyramidal geometry closely related to that of $[W_6I_{14}]^{2-}$ through formal removal of a $[WI]^{1-}$ moiety. Reaction with Zn reduces $[W_5I_{13}]^{1-}$ to $[W_5I_{13}]^{2-}$, which then undergoes terminal ligand displacement when reacted with $Ag(CF_3SO_3)$ to form $[W_5I_8(CF_3SO_3)_5]^{2-}$. Crystals of W_5I_{16} are encountered when Phase A is heated to 250 °C; their structure is characterized by one-dimensional chains composed of $[W_5I_{13}]^{1-}$ units linked by triiodide bridges. Heating Phase A at 300 °C in the presence of CsI yields a mixture of phases including CsW_5CI_{16}, containing the $[W_5(C)I_{13}]^{1-}$ carbide cluster in which the base of square-pyramidal $[W_5I_{13}]^{1-}$ is capped by a carbon atom (presumably originating from residual CO in Phase A). Cluster nucleation terminates at 550 °C with the formation of one- (W_6I_{18}) and two-dimensional (W_6I_{12} and W_6I_{16}) solids built up from octahedral $[W_6I_{14}]^{2-}$ cluster units, depending on the amount of iodine accompanying Phase B as a reactant. Incorporating KI in this reaction generates the dimensionally reduced product, which completely dissolves in ethanol and is precipitated as molecular $(Bu_4N)_2[W_6I_{14}]$ in good overall yield (30% based on $W(CO)_6$). Treatment of the latter with $Ag(CF_3SO_3)$ produces $[W_6I_8(CF_3SO_3)_6]^{2-}$, providing access to the ligand substitution chemistry of the $[W_6I_8]^{4+}$ core. The temperature-dependent isolation of the preceding binary tungsten iodides demonstrates the following reaction sequence, based upon which a specific nucleation pathway is proposed: $[W_3I_9]^{1-} \rightarrow [W_4I_{11}]^{1-} \rightarrow [W_5I_{13}]^{1-} \rightarrow [W_6I_{14}]^{2-}$.

Introduction

We have initiated chemical investigations intended to support the development of pharmaceutical agents with improved X-ray contrast imaging properites *in vivo*. Such drugs, with over 50 years of experimental experience,[1] represent mature technologies in diagnostic medical imaging. Nonetheless, a new class of X-ray contrast agents with improved radiological properties is desirable.[2] These agents can be based on mono- or polynuclear metal compounds, with a primary requirement that they manifest significant improvement in contrast enhancement over the barium- or iodine-based agents currently in clinical use. In this context, tungsten compounds, including those with additional high-Z absorbers (such as iodine), offer considerable promise. In addition to the favorable absorption properties of the element, low-valent tungsten halides show a pronounced tendency to form clusters, thereby providing enhanced absorption on a per mole dosage basis. Consequently, we have reexamined and substantially extended, in terms of new phases and synthetic accessibility, binary compounds of tungsten and iodine. Further, in the course of this research, we have uncovered structural evidence which lends direct support to a proposed pathway for the solid-state nucleation process culminating with the formation of octahedral $[W_6I_{14}]^{2-}$ clusters.

The syntheses of all previously known or claimed binary tungsten iodides[3–9] are recapitulated in Scheme 1. Nearly all useful results are those of Schäfer *et al.*[3–5] and Hogue and McCarley.[6] Despite the considerable number of entries in the scheme, only two products are structurally defined. Among binary phases, the compound W_6I_{12} has been obtained in an orthorhombic cell which from X-ray powder diffraction is isomorphous with that of Mo_6I_{12}.[3] The latter has been crystallographically related to Mo_6Cl_{12} whose structure has been determined by single-crystal methods.[3] Consequently, W_6I_{12} has the two-dimensional structure $[W_6I^i_8]I^a_2I^{a-a}_{4/2}$.[10] Evidence for the other phases is based on elemental analyses and/or crystallographic parameters different from those of W_6I_{12}.

[⊗] Abstract published in *Advance ACS Abstracts,* August 1, 1995.

(1) Strain, W. H. In *Contrast Media: Biological Effects and Clinical Application*; Parvez, Z., Moncada, R., Sovak, M., Eds.; CRC Press: Boca Raton, FL, 1987; Vol. 1, pp 3–13.

(2) Almén, T.; Berg, A.; Chang, C., *et al.* Contrast Media. PCT Application WO 92/17215; Salutar, Inc., March 27, 1992.

(3) Schäfer, H.; Schnering, H.-G.; Tillack, J.; Kuhnen, F.; Wöhrle, F.; Baumann, H. *Z. Anorg. Allg. Chem.* **1967**, *353*, 281.

(4) Schulz, H. G.; Siepmann, R.; Schäfer, H. *J. Less-Common Met.* **1970**, *22*, 136.

(5) Schäfer, H.; Schulz, H.-G. *Z. Anorg. Allg. Chem.* **1984**, *516*, 196.

(6) Hogue, R. D.; McCarley, R. E. *Inorg. Chem.* **1970**, *6*, 1354.

(7) Virmani, Y.; Barnes, D. S.; Skinner, H. A. *J. Chem. Soc., Dalton Trans.* **1974**, 399.

(8) Djordjevic, C.; Nyholm, R. S.; Pande, C. S.; Stiddard, M. H. B. *J. Chem. Soc. A* **1966**, 16.

(9) Westland, A. D.; Muriithi, N. *Inorg. Chem.* **1973**, *12*, 2356.

(10) Nomenclature: Schäfer, H.; Schnering, H.-G. *Angew. Chem.* **1964**, *76*, 833. See also ref 11.

(11) Lee, S. C.; Holm, R. H. *Angew. Chem., Int. Ed. Engl.* **1990**, *29*, 840.

0002-7863/95/1517-8139$09.00/0

Scheme 1. Reported Syntheses of Binary Tungsten–Iodine Solid Phases and Molecular Complexes

				ref.
• **Solid Phases**[a]				
$W + I_2$	(600°C)	→	W_6I_{12}	3
$W_6Cl_{12} + KI + LiI$	(540°C/EtOH/500°C)	→	W_6I_{12}	6
$WI_{3.2.3.3} + I_2$	(600/275°C)	→	W_6I_{12}	4,5
W_6I_{15}	(210°C)	→	W_6I_{14}	5
$W_6I_{12} + I_2$	(300°C)	→	W_6I_{15}	4,5
$W(CO)_6 + I_2$	(~530°C)	→	$WI_{2.7\text{-}2.8}$	7
$W_6I_{12} + I_2$	(200°C)	→	W_6I_{17} ($WI_{2.83}$)	5
$W + I_2$	(500/350°C)	→	$WI_{3.0}$	5
$W(CO)_6 + I_2$	(120°C)	→	$WI_{\sim 3}$[b]	8
$W(CO)_6 + I_2$	(120°C)	→	$WI_{3.2.3.3}$	4,5
$WCl_6 + HI$	(110°C)	→	WI_4	5
$W(CO)_6 + I_2$	(PhH/PhMe soln., 100°C)	→	WI_4	9
• **Molecular Complexes**[c]				
$W_6I_{12} + HI + I^-$	(EtOH soln.)	→	$[W_6I_{14}]^{2-}$	6
$W_6I_{12} + NaOH/ HI$	(aq. soln.)	→	$[W_6I_{12}(OH_2)_2]$	6
$W_6I_{12} + EtOH$	(EtOH soln.)	→	$[W_6I_{12}(EtOH)_2]$	6
$W_6I_{12} + HCl + Cl^-$	(EtOH soln.)	→	$[W_6I_{12}Cl_2]^{2-}$	6
$W_6I_{12} + HX$	(EtOH soln.)	→	$[W_6I_{11}X(EtOH)_2]$[d]	6
$W_6I_{12} + HX + X^-$	(EtOH soln.)	→	$[W_6I_8X_6]^{2-}$[e]	6

[a] The structure of *only* W_6I_{12} is supported by X-ray (powder) data.[3] [b] Variable composition. [c] The structure of *only* $(Bu_4N)_2[W_6I_{14}]$ is supported by single-crystal X-ray data.[12] [d] X = F^-, Cl^-, Br^-. [e] X = Cl^-, Br^-.

Among molecular species, the structure of $[W_6I_{14}]^{2-}$ has been established as $[W_6I^i_8I^a_6]^{2-}$ by a single-crystal study of its Bu_4N^+ salt.[12]

The $[W_6I_{14}]^{2-}$ clusters present in the foregoing tungsten(II) iodide compounds display a geometry common to a range of solid-state and solution species.[11] Without exception, these $[M_6X_{14}]^{n-}$ type cluster units (M = Nb, X = I;[13] M = Mo, X = Cl, Br, I, S, Se;[3,14] M = W, X = Cl, Br, I;[3,15] M = Tc, X = S, Se;[16] M = Re, X = S, Se, Te[16b,17]) originate from solid-state reactions at elevated temperatures. Their structure consists of a metal–metal bonded M_6 octahedron surrounded by eight face-capping X atoms (X^i) and six vertex-capping X atoms (X^a), as illustrated for $[Mo_6Cl_{14}]^{2-}$ in Figure 1. Typical of solid-state reactions, very little is known about the nucleation process leading to the formation of these clusters. In this respect, the most thoroughly studied system to date is that affording $[Mo_6Cl_{14}]^{2-}$ from monomeric Mo–Cl species in $AlCl_3$/KCl/$BiCl_3$/Bi melts at 306 °C.[18] Here, the process was interpreted as proceeding in two distinct steps, both of which were subjected to kinetics analysis. The first step was proposed to involve the formation of a pentanuclear chain of edge-sharing square-planar

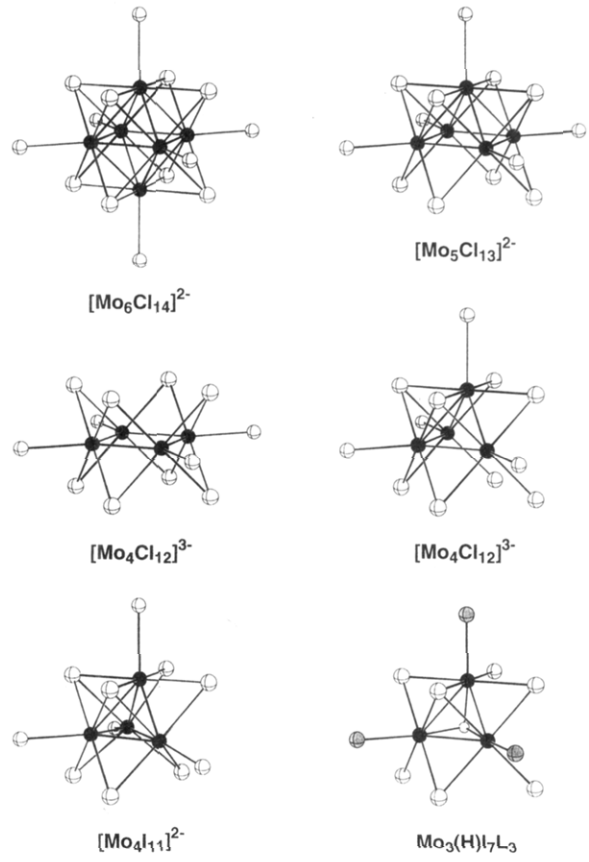

Figure 1. Idealized structures of $[Mo_6Cl_{14}]^{2-}$ and related clusters. Black, cross-haired white, gray, and open white spheres represent Mo, halogen, L, and H atoms, respectively. Square pyramidal $[Mo_5Cl_{13}]^{2-}$, square and butterfly $[Mo_4Cl_{12}]^{3-}$, distorted tetrahedral (or butterfly) $[Mo_4I_{11}]^{2-}$, and trigonal $Mo_3(H)I_7L_3$ geometries all derive from the face-capped octahedral $[Mo_6Cl_{14}]^{2-}$ parent. Structural similarities between clusters are best recognized by focusing on the cube of eight core halides.

$MoCl_4$ units which then collapses to form the $[Mo_5Cl_8]^{3+}$ core in an $[Mo_5Cl_{13}]^{2-}$ cluster. This intermediate was isolated and demonstrated to adopt the square-pyramidal structure shown at the upper right in Figure 1.[18,19] Consistent with their rather obvious structural relationship, the final step consists of incorporation of one Mo atom and one Cl atom in an "activated" $[Mo_5Cl_{13}]^{2-}$ cluster to form $[Mo_6Cl_{14}]^{2-}$.

Subsequent *solution* chemistry has produced a number of lower-nuclearity molybdenum-halide clusters with geometries extractable from the $[Mo_6Cl_{14}]^{2-}$ structure, which might be considered suggestive of a more complex nucleation process than that just described. The redox chemistry of $[Mo_5Cl_{13}]^{2-}$ has since been explored, resulting in the isolation of $[Mo_5Cl_{13}]^{1-,3-}$, which presumably retain the connectivity of their parent cluster; the analogous $[Mo_5Br_{13}]^{1-,2-,3-}$ clusters have also been prepared.[20] Two isomers of $[Mo_4Cl_{12}]^{3-} = [Mo_4Cl^i_8Cl^a_4]^{3-}$ with the structures depicted in Figure 1 have been synthesized starting from dinuclear $Mo_2Cl_4(PPh_3)_2(MeOH)_2$.[21] The square and butterfly geometries of these clusters are formally derived from $[Mo_6Cl_{14}]^{2-}$ through removal of two $[MoCl]^{1+,0}$ fragments at *trans* and *cis* octahedral apices, respectively. A closely related butterfly cluster $[Mo_4(O)Br_{12}]^{2-}$, in which the wingtips are spanned by a capping μ_4-O atom, has been prepared from

(12) Zietlow, T. C.; Schaefer, W. P.; Sadeghi, B.; Hua, N.; Gray, H. B. *Inorg. Chem.* **1986**, *25*, 2195.
(13) (a) Bateman, L. R.; Blount, J. F.; Dahl, L. F. *J. Am. Chem. Soc.* **1966**, *88*, 1082. (b) Simon, A.; Schnering, H. G.; Schäfer, H. *Z. Anorg. Allg. Chem.* **1967**, *355*, 295. (c) Imoto, H.; Corbett, J. D. *Inorg. Chem.* **1980**, *19*, 1241.
(14) (a) Chevrel, R.; Sergent, M.; Prigent, J. *J. Solid State Chem.* **1971**, *3*, 515. (b) Bars, O.; Guillevic, J.; Grandjean, D. *J. Solid State Chem.* **1973**, *6*, 48. (c) Fischer, O. *Appl. Phys.* **1978**, *16*, 1.
(15) Schäfer, H.; Siepmann, R. *Z. Anorg. Allg. Chem.* **1968**, *357*, 273.
(16) (a) Bronger, W.; Kanert, M.; Loevenich, M.; Schmitz, D.; Schwochau, K. *Angew. Chem., Int. Ed. Engl.* **1993**, *32*, 576. (b) Bronger, W.; Kanert, M.; Loevenich, M.; Schmitz, D. *Z. Anorg. Allg. Chem.* **1993**, *619*, 2015.
(17) (a) Spangenberg, M.; Bronger, W. *Angew. Chem., Int. Ed. Engl.* **1978**, *17*, 368. (b) Bronger, W.; Miessen, H.-J.; Neugröschel, R.; Schmitz, D.; Spangenberg, M. *Z. Anorg. Allg. Chem.* **1985**, *525*, 41. (c) Klaiber, F.; Petter, W.; Hulliger, F. *J. Solid State Chem.* **1983**, *46*, 112.
(18) Jödden, K.; Schäfer, H. *Z. Anorg. Allg. Chem.* **1977**, *430*, 5.
(19) Jödden, K.; Schnering, H. G.; Schäfer, H. *Angew. Chem., Int. Ed. Engl.* **1975**, *14*, 570.
(20) Zietlow, T. C.; Gray, H. B. *Inorg. Chem.* **1986**, *25*, 631.
(21) Aufdembrink, B. A.; McCarley, R. E. *J. Am. Chem. Soc.* **1986**, *108*, 2474.

$MoBr_3 \cdot 3H_2O$.[22] Folding the butterfly geometry such that the two proximal terminal halide atoms fuse produces a structure adopted by $[Mo_4I_{11}]^{2-} = [Mo_4I^i_7I^a_4]^{2-}$,[23] as shown in Figure 1. Consequently, this cluster, which was synthesized by reaction of monomeric $[Mo(CO)_4I_3]^{1-}$ with I_2,[23a] can be viewed as a rearranged fragment of $[Mo_6I_{14}]^{2-}$. Finally, trinuclear clusters $Mo_3(H)I_7L_3$ (L = THF, MeCN, PhCN, PEt_3, PPh_3), with the triangular geometry displayed in Figure 1, have been obtained from reactions of $Mo(CO)_3(THF)_3$ with I_2 in solution.[24] This structure may also be derived from $[Mo_6I_{14}]^{2-}$ by extracting an $[Mo_3I_4]^{2-}$ fragment (composed of three *cis* [MoI] moieties and their attendant μ_3-I atom), replacing the three remaining terminal iodides with neutral ligands L, and capping the exposed face with a μ_3-H atom.

Although the existence of the tri- and tetranuclear clusters in Figure 1 would seem to implicate some or all of them in the solid-state nucleation of $[Mo_6X_{14}]^{2-}$, no direct evidence to that effect has yet come to light. Despite their structural similarities, the conversion of one geometry into another has only been accomplished in the case of $[Mo_5Cl_{13}]^{2-} \rightarrow [Mo_6Cl_{14}]^{2-}$.[18] We report here direct structural evidence for the following sequence of conversions in the solid-state nucleation of the analogous $[W_6I_{14}]^{2-}$ clusters: $[W_3I_9]^{1-} \rightarrow [W_4I_{11}]^{1-} \rightarrow [W_5I_{13}]^{1-} \rightarrow [W_6I_{14}]^{2-}$. In addition, the preparation, properties, and chemistry of phases containing these and related tungsten−iodine cluster species are described in full detail.

Experimental Section

Preparation of Compounds. The compounds $W(CO)_6$ (Strem), iodine (Strem), $(R_4N)I$ (R = Pr, Bu; Aldrich), $(Ph_4P)I$ (Aldrich), and $Ag(CF_3SO_3)$ (Aldrich) were used without further purification. Both $W(CO)_6$ and iodine were ground with a mortar and pestle prior to use. Solvents were distilled from the appropriate drying agent and degassed prior to use. Solid-state reactions were performed in Pyrex tubes with dimensions i.d. × o.d. × *l* = 13 × 19 × 260 mm. Except for the preparations of $(Pr_4N)[W_5I_{13}]\cdot THF$, $(Bu_4N)[W_5(C)I_{13}]$, and $(Bu_4N)_2[W_6I_{14}]$, reactions in solution were carried out under a pure dinitrogen atmosphere using standard Schlenk techniques.

Phase A. An intimate mixture of 2.0 g (5.7 mmol) of $W(CO)_6$ and 10 g (39 mmol) of I_2 was added to a Pyrex tube, degassed, and connected to an oil bubbler. The reaction mixture was heated in an oil bath at 140 °C until the evolution of CO ceased (*ca.* 3 h). The resulting black-gray solid (Phase A) was removed from the tube and pulverized. The solid was washed repeatedly with ether until the filtrate became colorless (*ca.* 300 mL), at which point 1.8 g of black solid (washed Phase A) remained.

$(Bu_4N)[W_3I_9]$. Washed Phase A (1.8 g) was added to 200 mL of THF and stirred overnight. The solution was filtered through Celite, and solid $(Bu_4N)I$ (0.50 g, 1.4 mmol) was added to the deep red filtrate. The solution was stirred for an additional 8 h and concentrated to *ca.* 5 mL under reduced pressure. The solution was layered with 25 mL of ether and maintained at −15 °C overnight. The resulting red-brown solid was filtered and washed quickly with 10 mL of ethanol. The solid was then washed with ether (3 × 10 mL), dried under vacuum, and recrystallized by slow evaporation of a dichloromethane solution to yield 0.38 g (11% based on $W(CO)_6$) of red-black crystalline product. Absorption spectrum (THF): λ_{max} (ϵ_M) 278 (30 400), 308 (15 000), 337 (sh, 12 300), 428 (sh, 8130), 455 (sh, 8860), 510 (4730), 604 (sh, 1060), 721 (468) nm. Anal. Calcd for $C_{16}H_{36}I_9NW_3$: C, 9.93; H, 1.87; I, 58.99; N, 0.72; W, 28.49. Found: C, 10.03; H, 1.93; I, 58.92; N, 0.75; W, 28.32.

W_4I_{13}. The Pyrex tube containing Phase A was sealed under vacuum, heated in a tube furnace at 165 °C for 50 h, and cooled to room temperature at a rate of 0.2 °C/min. The tube was opened (see Caution 1), and the contents were removed and washed with aliquots of ether to remove unreacted iodine. The black solid was then washed with THF (5 × 50 mL) and more ether (3 × 5 mL), leaving 0.30 g (8.8% based on $W(CO)_6$) of black microcrystalline product. Anal. Calcd for $I_{13}W_4$: I, 69.17; W, 30.83. Found: I, 69.51; W, 30.41. *Caution 1: Although the majority of the CO is expelled in the synthesis of Phase A, the reaction tube is highly pressurized with CO when removed from the furnace. To minimize blowout, the tube is carefully scored with a metal file and wrapped inside thick foam rubber tubing. The tube is then opened in a well-ventilated hood behind a shield by striking it carefully once with a hammer.*

Phase B. The Pyrex tube containing Phase A was sealed under vacuum and heated in a tube furnace at 200 °C for 50 h; it was then cooled (0.2 °C/min) to room temperature. The tube was opened (see Caution 1) and its contents were removed and pulverized. The black-gray solid (unwashed Phase B) was washed with 200-mL aliquots of ether to remove unreacted iodine. When the filtrates became colorless, 2.1 g of a dark blue-black solid (Phase B) remained.

$(Pr_4N)[W_5I_{13}]\cdot THF$. Phase B (1.75 g) was added to 200 mL of ethanol over the course of 30 min. The dark green suspension was stirred for 18 h at room temperature, during which time all the solid dissolved. Excess $(Pr_4N)I$ (0.50 g, 1.6 mmol) was added as a solid to the solution, causing an immediate precipitation of a blue solid. The solution was stirred for 30 min; the solid was collected by filtration and washed with ethanol (15 mL) and ether (2 × 10 mL). The solid was dried under aspirator vacuum and recrystallized from THF/hexane at −15 °C to afford 0.98 g (31% based on $W(CO)_6$) of blue microcrystalline solid. Absorption spectrum (THF): λ_{max} (ϵ_M) 298 (33 700), 347 (sh, 13 900), 370 (sh 11 800), 423 (sh, 7720), 478 (5880), 524 (4990), 588 (4190), 623 (4080), 722 (2900), 844 (2050) nm. Anal. Calcd for $C_{16}H_{36}I_{13}NOW_5$: C, 6.79; H, 1.28; I, 58.34; N, 0.50; W, 32.53. Found: C, 6.48; H, 1.24; I, 58.84; N, 0.52; W, 32.79.

$(Pr_4N)_2[W_5I_{13}]$. A 100-mL Schlenk flask was charged with 1.0 g (0.35 mmol) of $(Pr_4N)[W_5I_{13}]\cdot THF$, 0.056 g (0.86 mmol) of Zn dust, and 0.22 g (0.70 mmol) of $(Pr_4N)I$. The contents of the flask were thoroughly degassed, and 30 mL of dichloromethane was added. The reaction mixture was stirred for 24 h, during which time a color change from deep green to brown-red was observed. The mixture was filtered through Celite and concentrated to *ca.* 3 mL under vacuum. The solution was layered with 10 mL of ether and maintained at −15 °C overnight. The reddish brown solid was collected by filtration, washed with ethanol (10 mL) and ether (2 × 10 mL), and dried in vacuum. This material was recrystallized from dichloromethane/ether to afford the product as 0.76 g (74%) of a microcrystalline black solid. Absorption spectrum (THF): λ_{max} (ϵ_M) 348 (12 500), 408 (sh, 7630), 535 (3760) nm. EPR (CH_2Cl_2, 120 K): axial, $g = 1.97$, peak-to-peak width 260 G. Anal. Calcd for $C_{24}H_{56}I_{13}N_2W_5$: C, 9.79; H, 1.92; I, 56.08; N, 0.95; W, 31.26. Found: C, 9.62; H, 1.85; I, 56.21; N, 0.92; W, 31.36.

$(Pr_4N)_2[W_5I_8(CF_3SO_3)_5]$. A mixture of 0.41 g (0.14 mmol) of $(Pr_4N)_2[W_5I_{13}]$ and 0.21 g (0.78 mmol) of $Ag(CF_3SO_3)$ was stirred in 35 mL of dichloromethane for 18 h in the absence of light. A gradual color change from brown-red to purple occurred and AgI precipitated. The reaction mixture was filtered through Celite, and the filtrate was concentrated to 5 mL under reduced pressure. Ether (25 mL) was carefully layered on top of the solution, resulting in the formation of black crystals over the course of 24 h. The crystalline product was collected and washed with 2 × 10 mL of ether to afford 0.22 g (51%) of pure product. Absorption spectrum (THF): λ_{max} (ϵ_M) 291 (sh, 11 600), 358 (sh, 6770), 439 (3960), 598 (1850) nm. The compound was identified by a single-crystal X-ray structure determination.

$(Bu_4N)[W_5(C)I_{13}]\cdot THF$. Cesium iodide (1.25 g, 4.81 mmol) was added to the Pyrex tube containing Phase A. The tube was then sealed under vacuum and heated in a steel-lined tube furnace at 300 °C (see Caution 2) for 50 h; it was then cooled (0.2 °C/min) to room temperature. The tube was opened (see Caution 1) and washed with 200 mL of ether to remove unreacted iodine. When the filtrates became colorless, 1.2 g of a brown-black partially crystalline solid remained. The FAB-MS of a dichloromethane-soluble portion of this solid

(22) Cotton, F. A.; Feng, X.; Shang, M.; Sun, Z. S. *Inorg. Chem.* **1993**, *32*, 1321.

(23) (a) Stensvad, S.; Helland, B. J.; Babich, M. W.; Jacobson, R. E.; McCarley, R. E. *J. Am. Chem. Soc.* **1978**, *100*, 6257. (b) Gordon, J. C.; Poli, R. *Acta Crystallogr.* **1995**, *C51*, 14.

(24) (a) Cotton, F. A.; Poli, R. *J. Am. Chem. Soc.* **1988**, *110*, 830. (b) Burini, A.; Cotton, F. A.; Czuchajowska, J. *Polyhedron* **1991**, *10*, 2145.

Table 1. Crystallographic Data[a] for W_4I_{13}, W_5I_{16}, W_6I_{12}, W_6I_{16}, W_6I_{18}, and CsW_5CI_{16}

	W_4I_{13}	W_5I_{16}	W_6I_{12}[b]	W_6I_{16}	W_6I_{18}	CsW_5CI_{16}
formula wt	2385.1	2949.7	2625.9	3133.5	3387.3	3094.6
crystal system	triclinic	orthorhombic	orthorhombic	monoclinic	monoclinic	triclinic
space group	$P\bar{1}$	$Pna2_1$	$Cmca$	$P2_1/c$	$P2_1/m$	$P\bar{1}$
Z	4	4	4	2	2	2
a, Å	10.822(3)	29.829(13)	15.856(5)	10.990(4)	10.469(3)	10.313(3)
b, Å	15.509(6)	10.275(6)	12.572(2)	10.709(3)	17.904(6)	10.426(3)
c, Å	16.232(5)	10.160(5)	12.579(3)	13.130(6)	10.512(4)	16.131(5)
α, deg	72.68(3)					103.06(2)
β, deg	81.75(3)			97.56(3)	118.86(2)	93.73(3)
γ, deg	81.06(3)					90.56(3)
V, Å^3	2555(2)	3114(3)	2508(1)	1532(1)	1726(1)	1685.4(9)
d_{calc}, g/cm^3	6.199	6.292	6.956	6.793	6.519	6.098
μ, mm^{-1}	33.637	34.260	42.171	38.552	36.012	32.713
R[c] (R_w[d]), %	8.05 (8.19)		6.26 (6.37)	5.34 (5.54)	4.12 (4.27)	6.00 (6.99)

[a] Obtained at 223 K with graphite monochromated Mo Kα (λ = 0.71073 Å) radiation. [b] T = 293 K. [c] $R = \sum||F_o| - |F_c||/\sum|F_o|$. [d] $R_w = \{\sum[w(|F_o| - |F_c|)^2]/\sum[w|F_o|^2]\}^{1/2}$.

Table 2. Crystallographic Data[a] for $(Bu_4N)[W_3I_9]$, $(Pr_4N)[W_5I_{13}]$·THF, $(Pr_4N)_2[W_5I_{13}]$, $(Bu_4N)[W_5(C)I_{13}]$·THF, $(Pr_4N)_2[W_5I_8(CF_3SO_3)_5]$, and $(Ph_4P)_2[W_6I_8(CF_3SO_3)_6]$·$CH_2Cl_2$

	$(Bu_4N)[W_3I_9]$	$(Pr_4N)[W_5I_{13}]$·THF	$(Pr_4N)_2[W_5I_{13}]$	$(Bu_4N)[W_5(C)I_{13}]$·THF	$(Pr_4N)_2[W_5I_8(CF_3SO_3)_5]$	$(Ph_4P)_2[W_6I_8(CF_3SO_3)_6]$·$CH_2Cl_2$
formula	$C_{16}H_{36}I_9W_3$	$C_{16}H_{36}I_{13}NOW_5$	$C_{24}H_{56}I_{13}N_2W_5$	$C_{21}H_{45}I_{13}NOW_5$	$C_{29}H_{56}F_{15}I_8N_2O_{15}S_5W_5$	$C_{55}H_{42}Cl_2F_{18}I_8O_{18}P_2S_6W_6$
formula wt	1936.1	2827.4	2941.7	2895.6	3052.5	3776.4
crystal system	monoclinic	triclinic	triclinic	monoclinic	triclinic	triclinic
space group	$P2_1/c$	$P\bar{1}$	$P\bar{1}$	$P2_1/n$	$P\bar{1}$	$P\bar{1}$
Z	4	2	2	4	2	2
a, Å	13.209(4)	9.925(2)	13.570(4)	11.128(3)	12.833(3)	13.780(4)
b, Å	14.771(4)	15.386(6)	13.764(3)	15.554(4)	14.898(4)	16.292(5)
c, Å	19.711(7)	17.265(7)	17.289(4)	28.336(6)	20.737(5)	22.361(7)
α, deg		79.77(3)	69.10(2)		69.67(2)	94.01(2)
β, deg	108.91(3)	73.96(3)	88.44(2)	95.36(2)	85.85(2)	107.54(2)
γ, deg		80.00(3)	65.34(2)		69.13(2)	112.26(2)
V, Å^3	3638(2)	2472(2)	2713(1)	4883(2)	3468(2)	4333(2)
d_{calc}, g/cm^3	3.535	3.799	3.600	3.878	2.923	2.895
μ, mm^{-1}	17.106	19.722	17.973	19.970	12.063	11.123
R (R_w),[b] %	5.11 (5.42)	6.38 (6.17)	4.27 (4.59)	4.60 (4.48)	8.03 (8.53)	4.71 (5.14)

[a] Obtained at 223 K with graphite monochromated Mo Kα (λ = 0.71073 Å) radiation. [b] For definitions *cf.* Table 1.

revealed the presence of $Cs[W_5(C)I_{13}]$, $Cs_2[W_6I_{14}]$, and cesium iodides that could not be fully identified. The black solid was stirred overnight in 150 mL of acetonitrile to give a deep orange solution. The solution was filtered, and 0.75 g (2.0 mmol) of solid $(Bu_4N)I$ was added to the filtrate. The red precipitate which immediately separated was collected by filtration and washed with ether (2 × 10 mL). The filtrate was evaporated to dryness to give a red-orange solid residue. The combined solids were partially dissolved in 50 mL of THF and the solution was filtered. The undissolved red solid was washed with ethanol (5 × 10 mL) and recrystallized from THF/hexane to give the product as 0.18 g (5.5% based on $W(CO)_6$) of a red microcrystalline solid. Absorption spectrum (THF): λ_{max} (ϵ_M) 329 (sh, 33,900), 403 (sh, 11,200), 442 (9830) nm. Anal. Calcd for $C_{21}H_{44}I_{13}NOW_5$: C, 8.71; H, 1.53; I, 56.97; N, 0.48; W, 31.75. Found: C, 8.54; H, 1.46; I, 57.06; N, 0.49; W, 31.68. *Caution 2: There is some risk of explosion when heating Phase A in a sealed Pyrex tube at 300 °C. Consequently, it is advised that the tube furnace be located in a well-ventilated explosion-proof hood. A steel-lined process tube is also recommended to minimize furnace damage in the event of an explosion. Heating at temperatures above 300 °C, changing the dimensions of the Pyrex tube, or scaling up the reaction may all result in explosions, and are cautioned against.*

W_6I_{12}. Phase B (0.62 g) was sealed in a Pyrex tube under vacuum and heated in a tube furnace at 550 °C for 50 h. The tube was cooled to room temperature at a rate of 0.2 °C/min and opened. The product as 0.23 g (25% based on $W(CO)_6$) of an orange solid is deposited at one end of the tube and some free iodine is found at the other end. The compound was identified by a single-crystal X-ray structure determination, and subsequent X-ray powder diffraction patterns.

W_6I_{16}. Unwashed Phase B (8.0 g) was sealed in a Pyrex tube under vacuum. The tube was heated in a tube furnace at 550 °C for 50 h and then cooled to room temperature at a rate of 0.2 °C/min. The tube was opened and the reaction product was washed with 100 mL of ether. The product was obtained as 1.3 g (44% based on $W(CO)_6$) of red-brown solid. The compound was identified by a single-crystal X-ray structure determination and subsequent X-ray powder diffraction patterns.

$(Bu_4N)_2[W_6I_{14}]$. Phase B (1.6 g) and KI (1.0 g, 6.0 mmol) were sealed under vacuum in a Pyrex tube and heated at 550 °C for 65 h. The tube was cooled to room temperature (0.2 °C/min) and opened. The black-orange product was completely dissolved in 125 mL of ethanol to give a deep orange solution, which was filtered. Addition of 0.50 g (1.4 mmol) of $(Bu_4N)I$ to the filtrate caused the immediate precipitation of a yellow-orange solid. This material was collected by filtration and washed with cold ethanol (2 × 10 mL) and ether (10 mL). The product was obtained as 0.95 g of a yellow-orange solid; the yield is 30% based on $W(CO)_6$ used in the preparation of Phase A. FAB-MS: *m/z* 3122 ($[(Bu_4N)(W_6I_{14})]^{1-}$), *m/z* 2881 ($[HW_6I_{14}]^{1-}$). Unit cell parameters obtained from a single crystal match those reported previously for this compound.[12]

$(Bu_4N)_2[W_6I_8(CF_3SO_3)_6]$. A mixture of 250 mg (0.074 mmol) of $(Bu_4N)_2[W_6I_{14}]$ and 135 mg (0.525 mmol) of $Ag(CF_3SO_3)$ in 30 mL of dichloromethane was stirred for 18 h in the absence of light and filtered through Celite to remove AgI. The bright yellow filtrate was concentrated to *ca.* 3 mL under reduced pressure; 20 mL of ether was carefully layered on top of the solution. Bright yellow crystals separated within hours; these were filtered and washed with ether (3 × 10 mL) to afford 0.21 g (81%) of pure product. Absorption spectrum (CH_2Cl_2): λ_{max} (ϵ_M) 289 (12 000), 343 (sh, 4830) nm. Anal. Calcd for $C_{38}H_{72}F_{18}I_8N_2O_{18}S_6W_6$: C, 13.04; H, 2.07; F, 9.78; I, 29.03; N, 0.84; S, 5.49; W, 31.56. Found: C, 13.08; H, 2.05; F, 9.65; I, 28.91; N, 0.86; S, 5.38; W, 31.42.

X-ray Data Collection and Reduction. Structures were determined for the compounds listed in Tables 1 and 2. Crystals of $(Bu_4N)[W_3I_9]$ (red-black blocks) were obtained by slow evaporation of a concentrated THF solution. Crystals of W_4I_{13} (black, irregular), CsW_5CI_{16} (black, irregular), W_6I_{12} (dark orange blocks), W_6I_{16} (red-black rhombic plates),

and W_6I_{18} (black rods) were picked from solid-state reaction products. X-ray quality crystals of $(Pr_4N)[W_5I_{13}]$·THF (black rectangular rods) and $(Bu_4N)[W_5(C)I_{13}]$·THF (brown-black rhombic prisms) were obtained by anaerobic vapor diffusion of hexane into a concentrated THF solution of the reaction product. Single crystals of $(Pr_4N)_2[W_5I_8(CF_3SO_3)_5]$ (black rhombic plates) were obtained directly from the reaction mixture. Suitable crystals of $(Pr_4N)_2[W_5I_{13}]$ (brown-black blades) and $(Ph_4P)_2[W_6I_8(CF_3SO_3)_6]$·$CH_2Cl_2$ (yellow plates) were obtained by diffusion of ether into dichloromethane solutions. The latter compound was obtained by a procedure analogous to that for the $(Bu_4N)^+$ salt, whose structure was determined and found to contain highly disordered triflate ligands. Single crystals were coated with Apiezon L grease and attached to glass fibers. The crystals were then transferred to a Nicolet R3m/V diffractometer and cooled in a dinitrogen stream to −50 °C.

Lattice parameters were obtained from least-squares analysis of more than 30 carefully centered reflections. Decay corrections were based on the measured intensities of reflections monitored periodically throughout the course of data collection; none of the crystals showed significant decay. The raw intensity data were converted (including corrections for scan speed, background, and Lorentz and polarization effects) to structure factor amplitudes and their esd's using the program XDISK from the SHELXTL PLUS software package. An empirical absorption correction based on the observed variation in intensity of azimuthal (Ψ) scans was applied to each data set using the program XEMP. For W_6I_{12} and W_6I_{16}, the absorption correction was improved by collecting excess data used to average equivalent reflections. Further details of the data collection are deposited.[25] Crystal data are collected in Tables 1 and 2.

Structure Solution and Refinement. Space group assignments were based on systematic absences, E statistics, and successful refinement of the structures. Structures were solved by direct methods (XS) with the aid of difference Fourier maps and were refined ($F_o > 6F_o$) with successive full-matrix least-squares cycles (XLS). Light atoms ($Z < 10$) were refined isotropically; all other atoms were refined anisotropically. Hydrogen atoms were not included in the final refinements except for those associated with the cations in $(Bu_4N)[W_3I_9]$, $(Pr_4N)[W_5I_{13}]$·THF, and $(Pr_4N)_2[W_5I_{13}]$. For these three cases, hydrogen atoms were fixed at ideal locations 0.96 Å from the bonded carbon atom and given a uniform value of U_{iso}. After the final cycle of refinement of each structure, all parameters had shifted by less than 1% of their esd, and the difference Fourier map showed no significant electron density. Structural data are summarized in Tables 1−6.[25]

The structure of $(Bu_4N)[W_5(C)I_{13}]$·THF exhibits a slightly disordered cluster core. One tungsten atom is disordered over two sites (*vide infra*) with crudely refined occupancy factors of 0.935 and 0.065. Its attendant terminal iodide ligand is similarly disordered with matching site occupancies. The expected corresponding disorder of the μ_4-C atom site involves a very small amount of electron density and consequently was not observed or modeled. For the less-occupied site, the W−I distance was constrained to be 2.80 Å. This constraint was necessitated by a conflict between the terminal iodide atom and one of the methyl groups of the $(Bu_4N)^+$ cation. As a further result, the methyl carbon atom had to be locked into position and displays an unusually large thermal parameter.

Other Physical Measurements. X-ray powder diffraction data were collected on a Scintag XDS-2000 diffractometer using Cu Kα radiation (λ = 1.5406 Å). Absorption spectra were measured with Cary Model 3 spectrophotometer. Cyclic voltammetry was performed with an EG&G Model 163 potentiostat, 0.1 M $(Bu_4N)(PF_6)$ supporting electrolyte, and a Pt disk working electrode. Potentials were determined vs an SCE reference electrode. EPR spectra were recorded at 120 K on a Bruker ESP 300-E spectrometer operating at X-band frequencies and employing a Bruker ER 412VT-E10 liquid nitrogen variable-temperature apparatus. FAB mass spectrometric measurements were performed on a JEOL SX-102 instrument.

Results and Discussion

The synthetic methods developed in this work which afford binary phases and/or molecular clusters with core units $[W_3I_6]^{2+}$, $[W_4I_7]^{3+}$, $[W_5I_8]^{3+,4+}$, $[W_5(C)I_8]^{4+}$, and $[W_6I_8]^{4+}$ are summarized in Scheme 2. A number of these compounds are obtained directly from sealed tube reaction or solubilization of two phases, which we designate as Phase A and Phase B. These materials have not been previously examined, although reactions between their precursors, $W(CO)_6$ and iodine, have been explored under different conditions (Scheme 1). Phase A is formed when $W(CO)_6$ and 7 equiv of iodine are heated at 140 °C, liberating CO; washing this solid with ether removes unreacted iodine, producing washed Phase A. Any residual CO present is too dilute to detect by infrared spectroscopy. As probed by X-ray powder diffraction, washed Phase A typically contains a small amount of insoluble crystalline W_4I_{13}, while its major components are amorphous. Due to its mixed nature, washed Phase A was not submitted for elemental analysis. However, similar materials produced in the reaction of $W(CO)_6$ and iodine at 120 °C have analyzed as $WI_{\sim 3}$.[1,2,5] Phase B is obtained directly from Phase A by heating it in a sealed tube for 50 h at 200 °C. The black-gray product is washed with ether to remove unreacted iodine. Again, X-ray powder diffraction revealed the only crystalline component of Phase B to be occasional traces of W_4I_{13}; its primary constituent is amorphous.

Scheme 2. Synthesis of Binary Tungsten−Iodide Solid Phases and Molecular Complexes

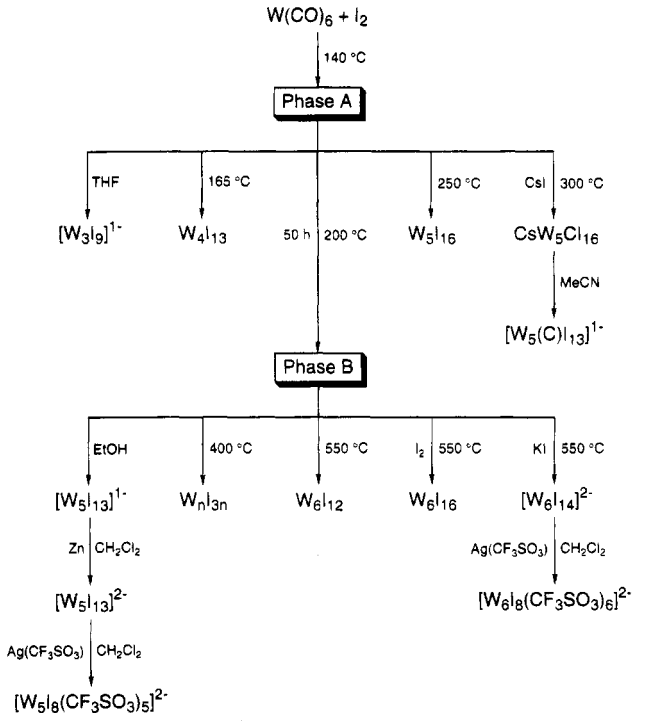

Trinuclear Cluster: $[W_3I_9]^{1-}$. Molecular $[W_3I_9]^{1-}$ is obtained directly from washed Phase A by stirring it in THF for 24 h and adding $(Bu_4N)I$ to the filtrate. The resulting solid is washed with ethanol to remove triiodide salts, a procedure which is best carried out quickly, as the cluster itself is slightly soluble in ethanol. The final product is recrystallized from dichloromethane to give a purified yield of 11%. The FAB mass spectrum of washed Phase A in THF exhibits major peaks corresponding to $[W_6I_{18}]^{1-}$, $[W_6I_{17}]^{1-}$, and $[W_6I_{16}]^{1-}$, suggesting that the solid precursor of $[W_3I_9]^{1-}$ contains the cluster in dimeric form. Consistent with this spectrum, one possible connectivity for the original solid is $[W_3I^t_6]I^aI^{a-a}{}_{1/2}(I_3)^{a-a}{}_{1/2}$·$xI_2$ = W_3I_{9+2x}, wherein two $[W_3I^t_6I^a]^{1+}$ units are linked via one μ_2-I and one μ_2-(I_3) to form a dimeric molecular entity. A similar type of bridging pattern is observed between clusters in one-dimensional W_6I_{18} (see Figure 11, below).

(25) See paragraph at the end of this article concerning supporting information.

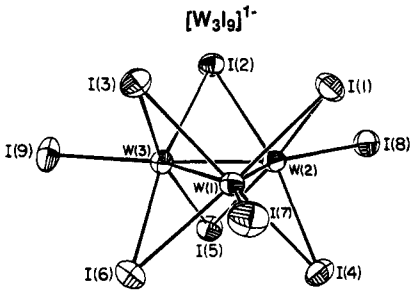

Figure 2. Structure of $[W_3I_9]^{1-}$ as the $(Bu_4N)^+$ salt; shown are 50% probability ellipsoids and the atom labeling scheme.

Table 3. Selected Interatomic Distances (Å) and Angles (deg) for $(Bu_4N)[W_3I_9]$

W(1)−W(2)	2.487(3)	W(1)−I(7)	2.811(4)	W(2)−I(8)	2.813(4)
W(1)−W(3)	2.477(3)	W(2)−W(3)	2.482(3)	W(3)−I(2)	2.754(3)
W(1)−I(1)	2.776(4)	W(2)−I(1)	2.767(4)	W(3)−I(3)	2.773(4)
W(1)−I(3)	2.769(3)	W(2)−I(2)	2.771(3)	W(3)−I(5)	2.790(4)
W(1)−I(4)	2.782(3)	W(2)−I(4)	2.780(3)	W(3)−I(6)	2.768(3)
W(1)−I(6)	2.776(4)	W(2)−I(5)	2.765(4)	W(3)−I(9)	2.821(4)
W(2)−W(1)−W(3)	60.0(1)		I(4)−W(2)−I(5)	89.1(1)	
W(2)−W(1)−I(1)	63.2(1)		W(1)−W(2)−I(8)	150.2(1)	
W(3)−W(1)−I(1)	105.3(1)		W(3)−W(2)−I(8)	149.8(1)	
W(2)−W(1)−I(3)	104.3(1)		I(1)−W(2)−I(8)	94.3(1)	
W(3)−W(1)−I(3)	63.5(1)		I(2)−W(2)−I(8)	94.7(1)	
I(1)−W(1)−I(3)	89.5(1)		I(4)−W(2)−I(8)	98.6(1)	
W(2)−W(1)−I(4)	63.4(1)		I(5)−W(2)−I(8)	97.4(1)	
W(3)−W(1)−I(4)	104.4(1)		W(1)−W(3)−W(2)	60.2(1)	
I(1)−W(1)−I(4)	88.8(1)		W(1)−W(3)−I(2)	105.4(1)	
I(3)−W(1)−I(4)	166.8(1)		W(2)−W(3)−I(2)	63.7(1)	
W(2)−W(1)−I(6)	105.2(1)		W(1)−W(3)−I(3)	63.4(1)	
W(3)−W(1)−I(6)	63.3(1)		W(2)−W(3)−I(3)	104.3(1)	
I(1)−W(1)−I(6)	167.6(1)		I(2)−W(3)−I(3)	88.9(1)	
I(3)−W(1)−I(6)	89.4(1)		W(1)−W(3)−I(5)	105.0(1)	
I(4)−W(1)−I(6)	89.5(1)		W(2)−W(3)−I(5)	63.0(1)	
W(2)−W(1)−I(7)	152.1(1)		I(2)−W(3)−I(5)	88.3(1)	
W(3)−W(1)−I(7)	147.9(1)		I(3)−W(3)−I(5)	166.8(1)	
I(1)−W(1)−I(7)	97.3(1)		W(1)−W(3)−I(6)	63.6(1)	
I(3)−W(1)−I(7)	94.7(1)		W(2)−W(3)−I(6)	105.6(1)	
I(4)−W(1)−I(7)	98.5(1)		I(2)−W(3)−I(6)	168.3(1)	
I(6)−W(1)−I(7)	95.1(1)		I(3)−W(3)−I(6)	89.4(1)	
W(1)−W(2)−W(3)	59.8(1)		I(5)−W(3)−I(6)	90.6(1)	
W(1)−W(2)−I(1)	63.5(1)		W(1)−W(3)−I(9)	150.1(1)	
W(3)−W(2)−I(1)	105.4(1)		W(2)−W(3)−I(9)	149.5(1)	
W(1)−W(2)−I(2)	104.6(1)		I(2)−W(3)−I(9)	97.5(1)	
W(3)−W(2)−I(2)	62.9(1)		I(3)−W(3)−I(9)	98.7(1)	
I(1)−W(2)−I(2)	90.7(1)		I(5)−W(3)−I(9)	94.5(1)	
W(1)−W(2)−I(4)	63.5(1)		I(6)−W(3)−I(9)	94.2(1)	
W(3)−W(2)−I(4)	104.3(1)		W(1)−I(1)−W(2)	53.3(1)	
I(1)−W(2)−I(4)	89.0(1)		W(2)−I(2)−W(3)	53.4(1)	
I(2)−W(2)−I(4)	166.7(1)		W(1)−I(3)−W(3)	53.1(1)	
W(1)−W(2)−I(5)	105.4(1)		W(1)−I(4)−W(2)	53.1(1)	
W(3)−W(2)−I(5)	64.0(1)		W(2)−I(5)−W(3)	53.1(1)	
I(1)−W(2)−I(5)	168.3(1)		W(1)−I(6)−W(3)	53.1(1)	
I(2)−W(2)−I(5)	88.5(1)				

Depicted in Figure 2 is the structure of $[W_3I_9]^{1-}$, which consists of an equilateral triangle of metal−metal bonded tungsten atoms with each edge bridged by two iodides (I(1−6)) and each vertex capped by a single iodide (I(7−9)). Interatomic distances and angles are listed in Table 3. The tungsten atoms are coordinated by iodine in a square-pyramidal geometry with mean distances of 2.773(4) for W−I^i and 2.815(4) for W−I^a. These square-pyramidal WI_5 units share basal edges comprising a cluster which closely approaches its idealized D_{3h} symmetry. The short intertungsten distances (mean = 2.482(3) Å) reflect the W−W bond order, which is greater than one, as might be expected for this 10-electron cluster.[26] The results of an extended Hückel calculation[27,28] applied to the idealized cluster are in agreement with this observation. Its metal-based frontier orbitals consist of a group of four primarily W−W bonding orbitals ($6a_1'$, $5a_2''$, and $8e'$) below the well-separated, fully-populated HOMO ($7a_1'$) which displays a mixture of W−W and W−I^i bonding character. The doubly-degenerate LUMO ($9e'$) is primarily metal-based and roughly nonbonding in character, and is chemically accessible, as witnessed by the cyclic voltammogram of $[W_3I_9]^{1-}$ in dichloromethane which reveals a quasireversible $[W_3I_9]^{1-/2-}$ couple at $E_{1/2} = -0.51$ V ($\Delta E_p = 210$ mV). The only other cluster with a core geometry similar to that of $[W_3I_9]^{1-}$ is $[Nb_3Cl_6(C_6Me_6)_3]^{1+}$; however, the Nb−Nb distances of 3.334(6) Å in this cluster are indicative of only very weak metal−metal interactions.[30]

Tetranuclear Cluster: W_4I_{13}. Varying amounts of this phase are observed in the reaction between $W(CO)_6$ and iodine at temperatures in the range 140−200 °C. A maximum yield of 8.8% is obtained at 165 °C. The other products formed at this temperature are readily removed by repeated washing with ether and THF. The remaining black solid is crystalline W_4I_{13}, which proved insoluble in common solvents and acids.

The compound forms molecular crystals in which two $[W_4I^i_7I^a_2]^{1+}$ units are linked by two triiodide ions. Two halves of such double clusters occur in the asymmetric unit; the halves of each double cluster are related by an inversion center. Shown in Figure 3 is an individual cluster and a bridged double cluster. The crystal also contains one molecule of iodine per double cluster molecule, affording the molecular formula $W_8I_{24}{\cdot}I_2$ ($WI_{3.25}$). The two independent clusters have very similar dimensions; because of the large number of independent metric parameters, the data in Table 4 and in the text are confined to those for the cluster in Figure 3.

The connectivity of the individual clusters is $[W_4I^i_7]I^a_2(I_3)^{a-a}{}_{2/2}$. Each $[W_4I_{11}]^{1-}$ cluster contains a $[W_4I^i_7]^{3+}$ core composed of a metal−metal bonded W_4 tetrahedron with two face-capping and five edge-bridging iodide atoms. Atoms W(1,2) are terminally coordinated by one iodide atom (I(8,9)) while W(3,4) are bound by one bridging triiodide atom I(10,11). Each WI_5 coordination unit is roughly square pyramidal. The W_4 tetrahedron is distorted, having one long, one intermediate, and four short bonds. The long bond is W(3)−W(4) (2.820(4) Å), whose atoms are spanned by μ_2-I(7) and are involved in the triiodide bridges. The intermediate bond is W(1)−W(2) (2.682(3) Å), the edge opposite the long bond. The short bonds are W(n)−W(3,4) (n = 1, 2), which average to 2.557(3) Å. Mean tungsten−iodine bond distances fall into the expected order W−I^a (2.76(1) Å) ≈ W−$I^i(\mu_2)$ (2.75(1) Å) < W−$I^i(\mu_3)$ (2.83(2) Å). The clusters with idealized symmetry C_{2v}, are bridged by two nearly linear, slightly unsymmetrical triiodide groups whose W−I bonds are the longest in the structure (mean 2.876 Å).

Other than W_6Br_{14}[31] and W_6Cl_{18},[32] W_4I_{13} is the only molecular binary tungsten−halide cluster phase. The component

(26) Based on a W−W single bond distance ($D(1)$) of 2.61 Å, Pauling's relation $D(n) = D(1) - 0.60 \log n$ predicts a W−W distance of 2.48 Å for $[W_3I_9]^{1-}$ (W−W bond order, n = 1.67), matching that observed. Pauling, L. *The Nature of the Chemical Bond*, 3rd ed.; Cornell University Press: Ithaca, NY, 1960; Chapter 7.

(27) (a) Hoffmann, R.; Lipscomb, W. N. *J. Chem. Phys.* **1962**, *36*, 2179, 3489. (b) Hoffmann, R. *J. Chem. Phys.* **1963**, *39*, 1397.

(28) These and subsequent calculations employed the program CACAO (PC version 4.0) with W and I parameters borrowed from other work (see ref 29): Mealli, C.; Proserpio, D. M. *J. Chem. Educ.* **1990**, *67*, 399.

(29) (a) Dedieu, A.; Albright, T. A.; Hoffmann, R. *J. Am. Chem. Soc.* **1979**, *101*, 3141. (b) Canadell, E.; Eisenstein, O. *Inorg. Chem.* **1983**, *22*, 2398.

(30) Churchill, M. R.; Chang, S. W.-Y. *J. Chem. Soc., Chem. Commun.* **1974**, 248.

(31) Sassmannshausen, J.; Schnering, H.-G. *Z. Anorg. Allg. Chem.* **1994**, *620*, 1312.

(32) Siepmann, R.; Schnering, H.-G.; Schäfer, H. *Angew. Chem., Int. Ed. Engl.* **1967**, *6*, 637.

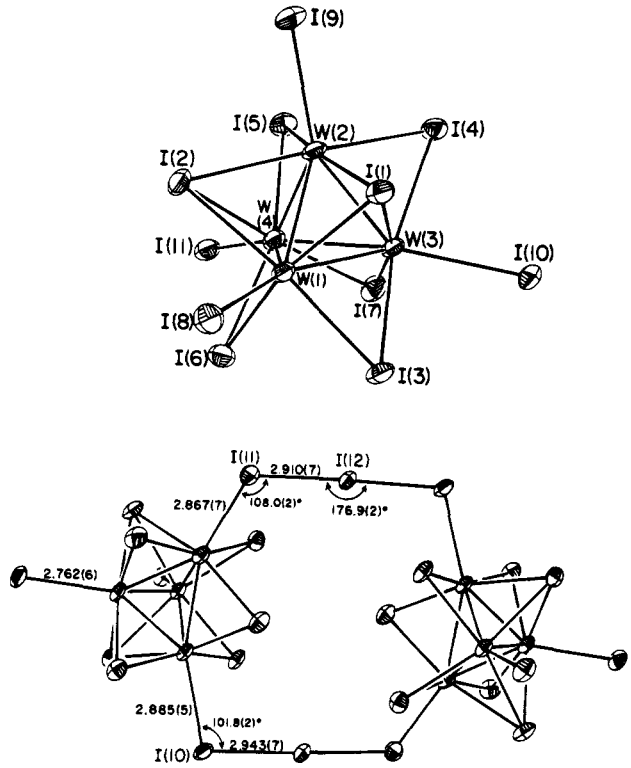

Figure 3. Upper: Structure of $[W_4I_{11}]^{1-} = [W_4I^i_7I^a_4]^{1-}$ cluster present in the phase W_4I_{13} and the atom labeling scheme. Lower: Structure of the phase $W_4I_{13} = [W_4I^i_7]I^a_2(I_3)^{a-a}{}_{2/2}{}^{\cdot i}/_2I_2$ showing the triiodide bridges between clusters, selected bridge bond distances and angles, and the bridge atom labeling scheme; the iodine molecule is omitted. The two clusters which form this dimer are related by an inversion center; atoms are depicted as 50% probability ellipsoids.

cluster $[W_4I_{11}]^{1-}$ contains 14 core electrons and tungsten in the 2.5+ oxidation state. A reduced structural analogue of these clusters, $[Mo_4I_{11}]^{2-}$, has been isolated in molecular form as its $(Bu_4N)^+$ and $(Ph_4P)^+$ salts.[23] This species shows a corresponding pattern of Mo–Mo bond distances but the "long" distance (3.035(5) Å) is 0.22 Å longer than in the tungsten cluster. While the latter effect may be associated with the additional electron, it seems clear that the long metal–metal bond of the tungsten cluster does not arise only as a consequence of triiodide bridge formation. As with $[Mo_4I_{11}]^{2-}$,[23] the structure of $[W_4I_{11}]^{1-}$ can be derived from $[W_6I_{14}]^{2-}$ by removal of two adjacent [WI] fragments and one core iodine atom and rearrangement of a second iodine to an edge midpoint position of the I_8 precursor cube.

Pentanuclear Clusters. When Phase B is completely dissolved in ethanol over the course of 18 h, a new cluster, $[W_5I_{13}]^{1-}$, has been isolated in molecular form as its $(Pr_4N)^+$ salt in 31% purified yield (based on $W(CO)_6$). A binary phase W_5I_{16} has been observed when Phase A was heated at somewhat higher temperatures (250–300 °C) than in the preparation of Phase B. Several crystals selected from the products of such reactions revealed a structure in which $[W_5I_8]^{4+}$ cores are linked via triiodides to form the one-dimensional chain shown in Figure 4. While the connectivity $[W_5I^i_8]I^a_3(I_3)^{a-a}{}_{2/2}{}^{\cdot}I_2$ of the phase is certain, the small size of the crystals produced prevented any successful correction of the data for absorption effects, and consequently a full structural refinement was not possible. In the usual preparation of Phase B at 200 °C, crystalline W_5I_{16} was never detected. The appearance of this phase at higher temperatures suggests its presence in amorphous form in the lower temperature preparations. We consider W_5I_{16} (or possibly $W_5I_{14}{\cdot}xI_2$) as the logical precursor to $[W_5I_{13}]^{1-}$; both species contain tungsten in the mean 2.4+ oxidation state. Indeed, paralleling Phase B, the material containing W_5I_{16} also yields $[W_5I_{13}]^{1-}$ when treated with ethanol and iodide. However, due to the increased likelihood of explosion at these higher temperatures (see Caution 2), amorphous Phase B remains the preferred source of $[W_5I_{13}]^{1-}$ and many other phases in Scheme 2.

(a) $[W_5I_{13}]^{1-,2-}$. The structure of $[W_5I_{13}]^{1-}$, presented in Figure 5 (upper), consists of a metal–metal bonded W_5 square pyramid whose triangular faces are capped by μ_3-I(1–4) and basal (b) edges are bridged by μ_2-I(5–8). Each tungsten site is terminally coordinated by one iodide (I(9–13)) to afford square-pyramidal WI_5 units. Overall, the cluster closely approaches C_{4v} symmetry. Metric data are provided in Table 5; bond angles are organized under this symmetry. Basal atoms W(2–5) are planar and form an essentially perfect square with indistinguishable W–W distances (mean 2.669(4) Å) and W–W–W angles. Similarly, $W_b–W_{ax}–W_b$ angles are 60° within uncertainty; the mean $W_b–W_{ax}$ distance (2.677(10) Å) does not differ from the corresponding $W_b–W_b$ bond length.

The compound $(Pr_4N)[W_5I_{13}]$ is soluble in THF, dichloromethane, and acetone. When a deep-green solution in dichloromethane is treated with zinc metal over the course of 24 h, the solution changes to brown-red. Upon the addition of excess cation, the compound $(Pr_4N)_2[W_5I_{13}]$ is isolated in 74% purified yield. The compound is air-stable in solid form; it is soluble in THF, dichloromethane, acetone, and acetonitrile, but its solutions slowly oxidize in air to $[W_5I_{13}]^{1-}$. The structure of $[W_5I_{13}]^{2-}$ is shown in Figure 5 (lower); metric data are listed in Table 5.

The addition of one electron to $[W_5I_{13}]^{1-}$ does not result in a significant change in overall cluster stereochemistry in the dianion. However, small effects are found in certain W–W and W–I bond distances. Among these, the W_4 basal unit remains planar but assumes a slightly rectangular shape in which adjacent angles differ by 2.2–2.5° and opposite sides by *ca.* 0.03 Å. Compared to the monoanion, the mean $W_b–W_b$ and $W_b–W_{ax}$ bond lengths in the dianion exhibit marginally significant decreases of 2.623(15) Å (−0.046 Å) and 2.658(4) Å (−0.019 Å), respectively. There is a barely discernible lengthening of terminal W–I distances, mean values being 2.80(1) Å in the monoanion and 2.84(1) Å in the dianion, consistent with an increase in the effective radius of the tungsten atoms upon reduction to the average tungsten oxidation state of 2.2+. As the monoanion, $[W_5I_{13}]^{2-}$ closely approaches idealized C_{4v} symmetry.

The clusters $[W_5I_{13}]^{1-,2-}$ bear an obvious structural relationship to $[W_6I_{14}]^{2-}$ by removal of a $[WI]^{1-,0}$ fragment. Indeed, the mean W–W (2.671(5) Å) and $W–I^i$ (2.792(7) Å) bond lengths of the latter are very close to those in the pentanuclear clusters, underscoring the structural relationship between the $[W_5I_8]^{4+,3+}$ and $[W_6I_8]^{4+}$ cores. Further, $[W_5I_{13}]^{1-,2-}$ are isostructural with $[Mo_5Cl_{13}]^{2-}$.[18] Consistent with their structural congruency, the two pentanuclear clusters are interconverted by electrochemically reversible reactions. The cyclic voltammogram of $[W_5I_{13}]^{2-}$ in acetonitrile solution, shown in Figure 6, reveals the $[W_5I_{13}]^{1-/2-}$ couple at $E_{1/2} = +0.05$ V (ΔE_p = 59 mV) and the $[W_5I_{13}]^{2-/3-}$ couple at $E_{1/2} = -0.54$ V (ΔE_p = 60 mV). Despite a number of attempts, the cluster trianion has not been successfully isolated. The electron transfer series $[Mo_5X_{13}]^{1-/2-/3-}$ (X = Cl^-, Br^-) has been previously observed.[20] By a structural criterion, the mixed-valence $[W_5I_{13}]^{1-,2-}$ clusters are electronically delocalized. The EPR spectrum of the dianion exhibits a broad axial feature centered at $g = 1.97$ and no resolved hyperfine structure. The slight changes in

Table 4. Selected Interatomic Distances (Å) and Angles (deg) for W_4I_{13}[a]

W(1)−W(2)	2.682(3)	W(2)−W(3)	2.559(4)	W(3)−W(4)	2.820(4)	W(4)−I(5)	2.765(5)
W(1)−W(3)	2.558(3)	W(2)−W(4)	2.559(5)	W(3)−I(1)	2.841(6)	W(4)−I(6)	2.752(5)
W(1)−W(4)	2.553(4)	W(2)−I(1)	2.818(6)	W(3)−I(3)	2.735(5)	W(4)−I(7)	2.744(5)
W(1)−I(1)	2.815(6)	W(2)−I(2)	2.807(5)	W(3)−I(4)	2.746(5)	W(4)−I(11)	2.867(7)
W(1)−I(2)	2.807(5)	W(2)−I(4)	2.759(5)	W(3)−I(7)	2.735(7)	I(10)−I(12A)	2.943(7)
W(1)−I(3)	2.751(5)	W(2)−I(5)	2.761(6)	W(3)−I(10)	2.885(5)	I(11)−I(12)	2.910(7)
W(1)−I(6)	2.772(6)	W(2)−I(9)	2.762(6)	W(4)−I(2)	2.861(5)	I(25)−I(26)[b]	2.753(9)
W(1)−I(8)	2.770(5)						

W(2)−W(1)−W(3)	58.4(1)	W(1)−W(2)−I(4)	119.9(1)	I(3)−W(3)−I(7)	94.7(2)
W(2)−W(1)−W(4)	58.5(1)	W(3)−W(2)−I(4)	62.1(1)	I(4)−W(3)−I(7)	96.8(2)
W(3)−W(1)−W(4)	67.0(1)	W(4)−W(2)−I(4)	104.4(2)	W(1)−W(3)−I(10)	142.4(2)
W(2)−W(1)−I(1)	61.6(1)	I(1)−W(2)−I(4)	86.4(2)	W(2)−W(3)−I(10)	140.8(2)
W(3)−W(1)−I(1)	63.6(1)	I(2)−W(2)−I(4)	166.6(2)	W(4)−W(3)−I(10)	153.4(2)
W(4)−W(1)−I(1)	115.7(1)	W(1)−W(2)−I(5)	120.0(2)	I(1)−W(3)−I(10)	99.7(2)
W(2)−W(1)−I(2)	61.5(1)	W(3)−W(2)−I(5)	105.8(2)	I(3)−W(3)−I(10)	84.4(1)
W(3)−W(1)−I(2)	115.8(1)	W(4)−W(2)−I(5)	62.5(1)	I(4)−W(3)−I(10)	82.7(1)
W(4)−W(1)−I(2)	64.3(1)	I(1)−W(2)−I(5)	167.5(2)	I(7)−W(3)−I(10)	94.2(2)
I(1)−W(1)−I(2)	104.7(2)	I(2)−W(2)−I(5)	85.7(2)	W(1)−W(4)−W(2)	63.3(1)
W(2)−W(1)−I(3)	119.7(1)	I(4)−W(2)−I(5)	82.4(2)	W(1)−W(4)−W(3)	56.6(1)
W(3)−W(1)−I(3)	61.9(1)	W(1)−W(2)−I(9)	129.8(2)	W(2)−W(4)−W(3)	56.6(1)
W(4)−W(1)−I(3)	104.7(2)	W(3)−W(2)−I(9)	146.6(2)	W(1)−W(4)−I(2)	62.2(1)
I(1)−W(1)−I(3)	85.7(2)	W(4)−W(2)−I(9)	146.5(2)	W(2)−W(4)−I(2)	62.1(1)
I(2)−W(1)−I(3)	167.2(2)	I(1)−W(2)−I(9)	91.0(2)	W(3)−W(4)−I(2)	106.4(2)
W(2)−W(1)−I(6)	119.8(2)	I(2)−W(2)−I(9)	90.4(2)	W(1)−W(4)−I(5)	124.8(2)
W(3)−W(1)−I(6)	105.5(2)	I(4)−W(2)−I(9)	97.0(2)	W(2)−W(4)−I(5)	62.3(2)
W(4)−W(1)−I(6)	62.1(1)	I(5)−W(2)−I(9)	95.9(2)	W(3)−W(4)−I(5)	98.9(1)
I(1)−W(1)−I(16)	167.2(2)	W(1)−W(3)−W(2)	63.2(1)	I(2)−W(4)−I(5)	84.6(2)
I(2)−W(1)−I(6)	85.9(2)	W(1)−W(3)−W(4)	56.4(1)	W(1)−W(4)−I(6)	62.9(1)
I(3)−W(1)−I(6)	82.9(2)	W(2)−W(3)−W(4)	56.6(1)	W(2)−W(4)−I(6)	125.4(2)
W(2)−W(1)−I(8)	129.9(2)	W(1)−W(3)−I(1)	62.6(1)	W(3)−W(4)−I(6)	99.2(1)
W(3)−W(1)−I(8)	146.2(2)	W(2)−W(3)−I(1)	62.7(1)	I(2)−W(4)−I(6)	85.2(1)
W(4)−W(1)−I(8)	146.8(2)	W(4)−W(3)−I(1)	106.9(1)	I(5)−W(4)−I(6)	161.1(2)
I(1)−W(1)−I(8)	90.8(2)	W(1)−W(3)−I(3)	62.5(1)	W(1)−W(4)−I(7)	105.0(2)
I(2)−W(1)−I(8)	90.8(1)	W(2)−W(3)−I(3)	125.1(1)	W(2)−W(4)−I(7)	106.4(2)
I(3)−W(1)−I(8)	96.5(1)	W(4)−W(3)−I(3)	98.3(1)	W(3)−W(4)−I(7)	58.9(1)
I(6)−W(1)−I(8)	96.3(2)	I(1)−W(3)−I(3)	85.5(2)	I(2)−W(4)−I(7)	165.2(2)
W(1)−W(2)−W(3)	58.4(1)	W(1)−W(3)−I(4)	125.2(1)	I(5)−W(4)−I(7)	98.3(2)
W(1)−W(2)−W(4)	58.2(1)	W(2)−W(3)−I(4)	62.6(1)	I(6)−W(4)−I(7)	95.5(2)
W(3)−W(2)−W(4)	66.9(1)	W(4)−W(3)−I(4)	98.1(1)	W(1)−W(4)−I(11)	145.7(1)
W(1)−W(2)−I(1)	61.5(1)	I(1)−W(3)−I(4)	86.2(2)	W(2)−W(4)−I(11)	138.9(1)
W(3)−W(2)−I(1)	63.6(1)	I(3)−W(3)−I(4)	163.2(2)	W(3)−W(4)−I(11)	151.7(2)
W(4)−W(2)−I(1)	115.5(1)	W(1)−W(3)−I(7)	105.2(2)	I(2)−W(4)−I(11)	101.7(2)
W(1)−W(2)−I(2)	61.5(1)	W(2)−W(3)−I(7)	106.7(2)	I(5)−W(4)−I(11)	79.5(2)
W(3)−W(2)−I(2)	115.8(1)	W(4)−W(3)−I(7)	59.2(1)	I(6)−W(4)−I(11)	86.9(2)
W(4)−W(2)−I(2)	64.2(1)	I(1)−W(3)−I(7)	166.0(2)	I(7)−W(4)−I(11)	93.2(2)
I(1)−W(2)−I(2)	104.7(2)				

[a] Data confined to one of the two inequivalent bridged clusters. [b] I_2 molecule.

metal−metal distances upon reduction of $[W_5I_{13}]^{1-}$ to the dianion are consistent with the results of extended Hückel calculations of $[Mo_5Cl_{13}]^{2-}$.[33] The MO occupied by the odd electron is essentially nonbonding and heavily metal in character. Calculations of the tungsten cluster by the same method afford an analogous energy level order and orbital character. The only other metal halide clusters with a square-pyramidal metal geometry are those in the $[Zr_5Cl_{12}H_4(PR_3)_5]$ series.[34] The $[Zr_5Cl_8H_4]^{4+}$ core consists of a Zr_5 square-pyramidal unit elaborated with eight edge-bridging chloride atoms and two face-capping and two edge-bridging hydride atoms.

(b) $[W_5(C)I_{13}]^{1-}$. When Phase A is reacted with excess CsI at 300 °C for 50 h, a brown-black solid mixture containing $[W_6I_{14}]^{2-}$, cesium iodides, and CsW_5CI_{16} (=$Cs[W_5(C)I_{13}]\cdot 1.5I_2$) is formed. A crystal of the latter was selected from the mixture and subjected to an X-ray structure determination. The crystal structure of this phase reveals it to be molecular in nature, containing individual $[W_5(C)I_{13}]^{1-}$ clusters; the asymmetric unit contains one cluster, one Cs^+, and one and one-half iodine molecules. A view of the structure selected to reveal cluster interactions with Cs^+ is provided in Figure 7; cluster dimensional data[25] are unimportantly different from those of the $(Bu_4N)^+$ cluster salt given below.

The cesium ion binds to the four μ_2-I atoms of one cluster at a mean bond distance of 3.87(1) Å and somewhat more tightly to four I^a atoms, each from a different cluster, at a mean distance of 3.76(3) Å. The CsI_8 coordination unit has a slightly distorted cubic arrangement with average I···I separations of 4.13(2) Å in the μ_2-I_4 face and 4.59(9) Å in the $I^a{}_4$ face; the remaining four cube edges vary in the range 4.23−4.65 Å. The dihedral angle between the μ_2-I_4 and $I^a{}_4$ mean planes is 4.1°. In its standard form, CsI crystallizes in the CsCl structure. Here the CsI_8 unit is exactly cubic, with a Cs−I distance of 3.955 Å and an I···I separation of 4.567 Å.[35] These values approach those of cesium coordination by the four μ_2-I atoms of a single cluster. This bonding mode raises the possiblity, currently being explored, of the cluster functioning as a tetradentate ligand in molecular complexes.

When the solid mixture is extracted with acetonitrile and the extract treated with $(Bu_4N)I$, the $(Bu_4N)^+$ salts of $[W_6I_{14}]^{2-}$ and

(33) Miessner, H.; Korol'kov, D. V. *Z. Anorg. Allg. Chem.* **1983**, *496*, 175.

(34) Cotton, F. A.; Lu, J.; Shang, M.; Wojtczak, W. A. *J. Am. Chem. Soc.* **1994**, *116*, 4364.

(35) Rymer, T. B.; Hambling, P. G. *Acta Crystallogr.* **1951**, *A4*, 565.

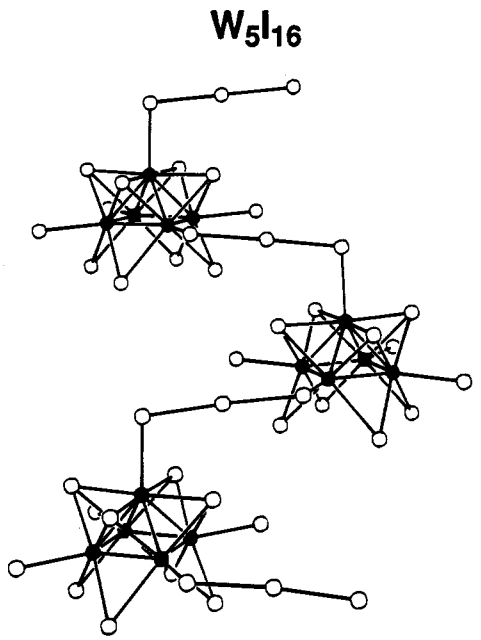

Figure 4. Structure of $W_5I_{16} = [W_5I^i_8]I^a_3(I_3)^{a-a}{}_{2/2}{\cdot}I_2$ showing triiodide bridges linking clusters in one-dimensional chains; iodine molecules are omitted.

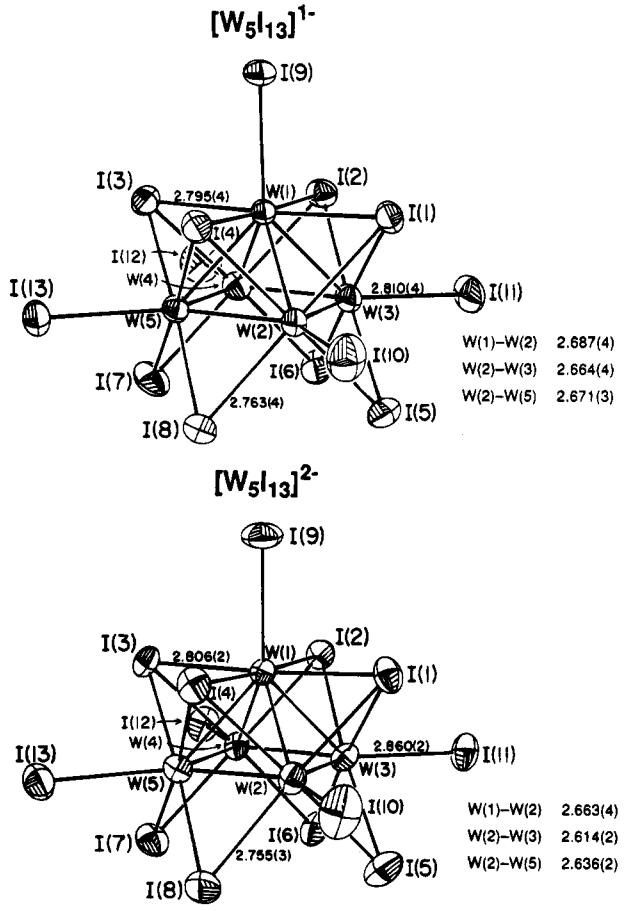

Figure 5. Upper: Structure of $[W_5I_{13}]^{1-}$ as the $(Pr_4N)^+$ salt, THF solvate. Lower: Structure of $[W_5I_{13}]^{2-}$ as the $(Pr_4N)^+$ salt. Shown are the atom labeling schemes, 70% probability ellipsoids, and selected W–I and W–W distances (Å).

$[W_5(C)I_{13}]^{1-}$ coprecipitate. Extraction of this material with THF followed by recrystallization of the residue from THF/hexane affords pure $(Bu_4N)[W_5(C)I_{13}]$ in 5.5% purified yield (based on $W(CO)_6$). Evidently, some residual CO is reductively cleaved in the course of formation of $[W_5(C)I_{13}]^{1-}$. A possible intermediate is $[W_5(CO)I_{13}]^{z-}$, formed in the reaction tube when highly pressurized with CO. The compound is soluble in THF, dichloromethane, and acetone. The structure of the carbide cluster is set out in Figure 8; selected bond distances and angles are included in Table 5 where they may be compared with those for $[W_5I_{13}]^{1-,2-}$. The cluster maintains the motif of the latter species, and its W_5 portion is nearly isometric. As mentioned above, the cluster itself is slightly disordered in the crystal, such that atoms W(4) and I(12) occasionally (*ca.* 6.5% of the time) occupy alternate positions matching those occupied by the additional atoms in $[W_6I_{14}]^{2-}$. This type of disorder was also occasionally observed in the crystals of various salts of $[W_5I_{13}]^{1-,2-}$ and underscores the regularity of their core I_8 cubes, as well as the close geometric relationship between these clusters and $[W_6I_{14}]^{2-}$. The carbon atom in $[W_5(C)I_{13}]^{1-}$ is somewhat irregularly bonded to the W(2–5) atoms at distances ranging from 2.09(4) to 2.24(3) Å and is located 1.06 Å below the plane of the W(2–5) square and 2.98 Å from the apical W(1) atom. All other structurally defined tungsten carbide clusters are tetranuclear with a butterfly geometry.[36] Metal–metal bonded $M_5(C)$ units have been previously encountered in $Fe_5(C)(CO)_{15}$,[37] the two isomers of $Ru_5(C)(CO)_{12}(C_6H_6)$,[38] $CpWRu_4(C)(CO)_{12}(CPh)$,[39] $[Os_5(C)(CO)_{14}]^{2-}$,[40] and $[Re_5(C)(H)(CO)_{16}]^{2-}$.[41] However, in all of these clusters, the carbon atom is μ_5 (residing approximately in the plane of the base of the M_5 square pyramid), and it appears to play more of an interstitial role than the base-capping μ_4-C atom in $[W_5(C)I_{13}]^{1-}$.

Hexanuclear Clusters. The first tungsten–halide clusters were prepared as the binary phases W_6X_{12} (X = Cl, Br, I) by Schäfer *et al.*[3] in 1967. These phases were found by X-ray powder diffraction to be isomorphous with Mo_6Cl_{12}, whose structure was determined by single-crystal methods.[3] The solids contain cubic $[W_6X_8]^{4+}$ core units with the connectivity $[W_6X^i_8]X^a_2X^{a-a}{}_{4/2}$; detailed structures have not been reported. In addition to being solubilized to yield pentanuclear clusters, Phase B can be heated at higher temperatures to afford W–I binary phases containing the $[W_6I_8]^{4+}$ core.

(a) W_6I_{12}. Maintenance of Phase B at 550 °C for 50 h results in the deposition of W_6I_{12} as an orange solid at one end of the reaction tube in 25% yield (based on $W(CO)_6$). The structure of W_6I_{12}, presented in Figure 9, makes evident its two-dimensional nature and the connectivity $[W_6I^i_8]I^a_2I^{a-a}{}_{4/2}$. Selected dimensional data are found in Table 6. The $[W_6I_8]^{4+}$ core has the familiar face-capped octahedral structure found for $[M_6X_8]^{z+}$ units with M = Mo and W. The metal–metal bonded octahedron has indistinguishable W–W (mean 2.665(3) Å) and W–(μ_3-I) (mean 2.795(6) Å) bond distances. Each bridging iodide atom is bonded to two tungsten atoms from different cores at 2.883(4) and 2.895(4) Å with a bridge angle of 134.3-(2)°. The two nonbridged iodide atoms are crystallographically equivalent ($W-I^a$ = 2.797(5) Å).

(b) W_6I_{16}. When unwashed Phase B is heated at 550 °C for 50 h and the resultant solid washed with ether, red-brown W_6I_{16}

(36) (a) Chisholm, M. H.; Hammond, C. E.; Johnston, V. J.; Streib, W. E.; Huffman, J. C. *J. Am. Chem. Soc.* **1992**, *114*, 7056. (b) Chisholm, M. H.; Johnston, V.; Martin, J. D.; Lobkovsky, E.; Huffman, J. C. *J. Cluster Sci.* **1993**, *4*, 105.

(37) Braye, E. H.; Dahl, L. F.; Hübel, W.; Wampler, D. L. *J. Am. Chem. Soc.* **1962**, *84*, 4633.

(38) Bailey, P. J.; Braga, D.; Dyson, P. J.; Grepioni, F.; Johnson, B. F. G.; Lewis, J.; Sabatino, P. *J. Chem. Soc., Chem. Commun.* **1992**, 177.

(39) Chiang, S.-J.; Chi, Y.; Su, P.-C.; Peng, S.-M.; Lee, G.-H. *J. Am. Chem. Soc.* **1994**, *116*, 11181.

(40) Johnson, B. F. G.; Lewis, J.; Nelson, W. J. H.; Nicholls, J. N.; Puga, J.; Raithby, P. R.; Rosales, M. J.; Schröder, M.; Vargas, M. D. *J. Chem. Soc., Dalton Trans.* **1983**, 2447.

(41) Henly, T. J.; Wilson, S. R.; Shapley, J. R. *Organometallics* **1987**, *6*, 2618.

Table 5. Selected Interatomic Distances (Å) and Angles (deg) for $[W_5I_{13}]^{1-,2-}$, $[W_5(C)I_{13}]^{1-}$, and $[W_5I_8(CF_3SO_3)_5]^{2-}$

	$[W_5I_{13}]^{1-}$	$[W_5I_{13}]^{2-}$	$[W_5(C)I_{13}]^{1-}$ [a]	$[W_5I_8(CF_3SO_3)_5]^{2-}$
W(1)−W(2)	2.687(4)	2.663(2)	2.690(2)	2.668(6)
W(1)−W(3)	2.684(3)	2.654(1)	2.701(2)	2.610(5)
W(1)−W(4)	2.667(3)	2.657(2)	2.686(2)	2.654(5)
W(1)−W(5)	2.671(3)	2.659(2)	2.695(2)	2.599(4)
W(1)−I(1)	2.779(4)	2.805(3)	2.763(3)	2.804(7)
W(1)−I(2)	2.798(5)	2.798(2)	2.778(3)	2.808(6)
W(1)−I(3)	2.795(4)	2.806(2)	2.782(3)	2.821(7)
W(1)−I(4)	2.772(5)	2.796(2)	2.785(3)	2.809(7)
W(1)−I(9)/O(1)	2.800(4)	2.816(2)	2.790(3)	2.13(6)
W(2)−W(3)	2.664(4)	2.614(2)	2.663(2)	2.594(5)
W(2)−W(5)	2.671(3)	2.636(2)	2.666(3)	2.601(5)
W(2)−C(1)			2.24(3)	
W(2)−I(1)	2.776(4)	2.797(2)	2.776(2)	2.779(5)
W(2)−I(4)	2.783(4)	2.808(2)	2.783(3)	2.777(4)
W(2)−I(5)	2.766(4)	2.776(2)	2.795(3)	2.762(8)
W(2)−I(8)	2.763(4)	2.755(3)	2.790(3)	2.738(6)
W(2)−I(10)/O(2)	2.809(5)	2.832(3)	2.788(4)	2.18(7)
W(3)−W(4)	2.672(3)	2.635(2)	2.663(3)	2.592(6)
W(3)−C(1)			2.14(3)	
W(3)−I(1)	2.787(4)	2.823(2)	2.767(3)	2.849(6)
W(3)−I(2)	2.781(5)	2.798(3)	2.764(3)	2.844(8)
W(3)−I(5)	2.756(5)	2.762(3)	2.800(3)	2.759(10)
W(3)−I(6)	2.768(5)	2.761(2)	2.801(3)	2.748(7)
W(3)−I(11)/O(3)	2.810(4)	2.860(2)	2.800(3)	2.14(5)
W(4)−W(5)	2.669(4)	2.607(2)	2.677(2)	2.588(5)
W(4)−C(1)			2.09(4)	
W(4)−I(2)	2.798(4)	2.801(2)	2.781(3)	2.780(5)
W(4)−I(3)	2.784(4)	2.799(2)	2.777(3)	2.792(7)
W(4)−I(6)	2.755(4)	2.761(2)	2.798(3)	2.778(7)
W(4)−I(7)	2.750(4)	2.772(2)	2.808(3)	2.764(6)
W(4)−I(12)/O(4)	2.790(6)	2.840(3)	2.787(4)	2.20(6)
W(5)−C(1)			2.18(3)	
W(5)−I(3)	2.776(5)	2.799(3)	2.776(3)	2.849(9)
W(5)−I(4)	2.777(4)	2.795(2)	2.777(3)	2.818(7)
W(5)−I(7)	2.748(4)	2.775(3)	2.793(3)	2.780(6)
W(5)−I(8)	2.750(5)	2.756(3)	2.789(3)	2.762(9)
W(5)−I(13)/O(5)	2.795(4)	2.838(2)	2.806(3)	2.11(3)
$W_b-W_{ax}-W_b$ [b]	59.5−60.0	58.7−59.5	59.2−59.7	58.9−59.2
mean of 4	59.8(2)	59.1(3)	59.4(2)	59.0(1)
$W_b-W_b-W_{ax}$	59.7−60.4	60.2−60.7	60.0−60.7	59.1−61.7
mean of 8	60.1(3)	60.4(2)	60.3(2)	60(1)
$W_b-W_b-W_b$	89.8−90.2	88.7−91.2	89.8−90.2	84.6−95.1
mean of 4	90.0(2)	90(1)	90.0(2)	90(5)
$W_{ax}-W_b-C$			73.7−76.1	
mean of 4			74.8(9)	
W_b-W_b-C			49.7−54.0	
mean of 8			52(2)	
$W-W-\mu_3$-I	60.9−61.7	61.4−62.8	60.7−61.6	60.9−63.9
mean of 24	61.3(3)	61.8(3)	61.1(2)	62.2(9)
$W_b-W_b-\mu_2$-I	60.8−61.3	61.4−62.1	61.2−61.7	61.3−62.6
mean of 8	61.1(2)	61.7(3)	61.5(2)	62.0(4)
W_b-C-W_b			74.2−78.0	
mean of 4			76(2)	
$W-\mu_3$-I−W	56.9−57.8	55.4−56.8	57.3−58.5	54.6−57.1
mean of 12	57.4(3)	56.4(5)	57.8(4)	55.6(9)
$W_b-\mu_2$-I−W_b	57.7−58.1	56.1−57.1	56.8−57.1	55.7−56.4
mean of 4	57.9(2)	56.6(4)	57.0(1)	56.0(3)
μ_3-I−W−μ_3-I	89.3−91.4	88.5−91.2	88.8−91.0	88.1−91.5
mean of 8	90.0(8)	90(1)	90.1(8)	90(1)
μ_2-I−W_b−μ_3-I	89.5−91.4	90.5−92.3	87.7−90.1	89.3−91.7
mean of 8	90.6(7)	91.3(7)	88.5(9)	90.4(8)
μ_2-I−W_b−μ_2-I	88.2−88.8	86.3−88.2	91.3−93.2	86.2−91.1
mean of 4	88.6(2)	87.3(9)	92.6(8)	89(2)
$I_aX/O_{ax}-W_{ax}-\mu_3$-I	87.0−90.4	87.8−89.5	88.5−89.9	86.2−89.7
mean of 4	89(1)	88.5(7)	89.2(5)	88(2)
I_b/O_b-W_b−I	87.0−90.1	86.2−89.9	86.7−89.1	82.1−91.8
mean of 16	88.8(8)	88.2(9)	87.8(6)	87(3)

[a] From $(Bu_4N)[W_5(C)I_{13}]$·THF. [b] Axial: W(1), I(9), O(1). Basal: W(2−5), I(10−13), O(2−5).

is obtained in 44% yield (based on $W(CO)_6$). The structure of this phase, set out in Figure 10, has the same two-dimensional connectivity as W_6I_{12} but contains between the sheets two iodine molecules per cluster. Unit cell parameters and X-ray powder diffraction data have been previously reported,[5] but the phase was incorrectly formulated as W_6I_{15} based on elemental analysis. The iodine-rich nature of this phase is attributed to free iodine present in unwashed Phase B. The phase W_6Br_{16} has been

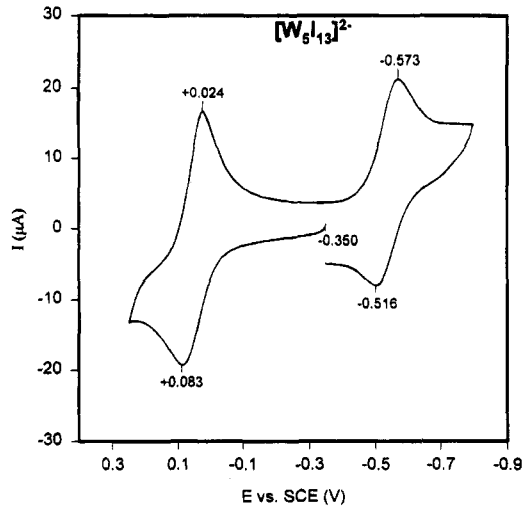

Figure 6. Cyclic voltammogram of $[W_5I_{13}]^{2-}$ in acetonitrile solution at 200 mV/s; peak potentials vs SCE are indicated.

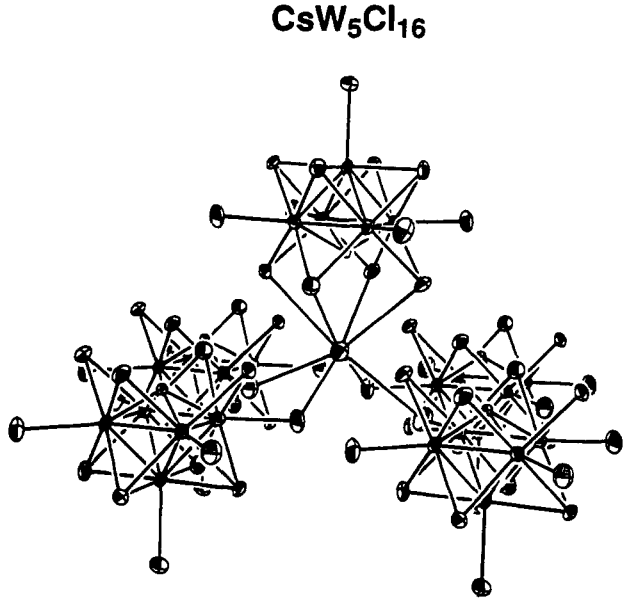

Figure 7. Structure of the molecular phase CsW_5Cl_{16}, presented with 70% probability ellipsoids in a perspective that emphasizes Cs–I interactions. Two of the five $[W_5(C)I_{13}]^{1-}$ clusters are partially eclipsed by two other clusters which are coplanar and are positioned in front of them. Iodine molecules are not shown. The ranges of Cs–I distances are 3.861(6)–3.891(6) Å to μ_2-I and 3.725(7)–3.788(6) Å to I^a (iodine atoms are designated as in an individual cluster).

prepared but is not isostructural with W_6I_{16}; clusters are linked by Br_4^{2-} polyanions in the connectivity pattern $[W_6Br^i_8]Br^a_4(Br_4)^{a-a}{}_{2/2}$.[42]

Selected metric parameters are collected in Table 6. Compared to W_6I_{12}, there are no significant differences in core distances or angles. Clusters are bridged with slightly longer W–(μ_2-I) interactions (2.893(3), 2.911(3) Å) and a more acute bridge angle (122.3(1)°). The packing of molecular iodine in the crystal causes some relative rotation of clusters, evident in a non-parallel alignment of W–I^a bond vectors and affording a "rippled" sheet structure. The clusters present in W_6I_{12} and W_6I_{16} contain W^{2+} and 24 electrons utilized in the 12 W–W core bonds.

(c) W_6I_{18}. When unwashed Phase B is heated in the range 400–500 °C, mixtures containing W_6I_{12}, W_6I_{16}, and a new

(42) Siepmann, R.; Schnering, H.-G. *Z. Anorg. Allg. Chem.* **1968**, *357*, 289.

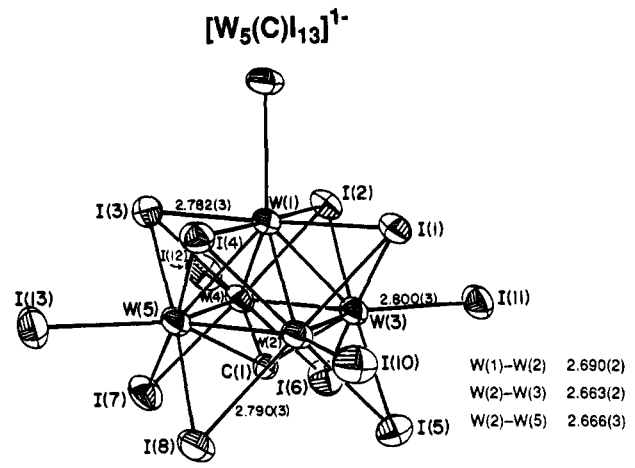

Figure 8. Structure of $[W_5(C)I_{13}]^{1-}$ as the $(Bu_4N)^+$ salt, THF adduct; shown are 50% probability ellipsoids and the atom labeling scheme.

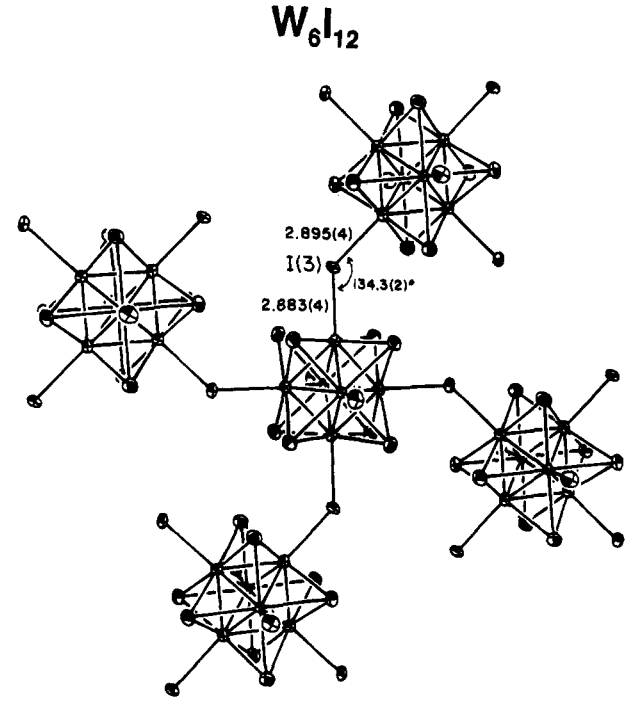

Figure 9. The structure of the two-dimensional phase $W_6I_{12} = [W_6I^i_8]I^a_2I^{a-a}{}_{4/2}$ showing iodide bridges between clusters and the bridge angle and distances. The view is down a 2-fold rotation axis (along W–I^a) perpendicular to a mirror plane. Atoms are depicted as 70% probability ellipsoids.

phase, black W_6I_{18} (WI_3), are produced at the hot end of the tube. Crystals of the latter phase are sometimes observed when tungsten metal and iodine are heated at 600–800 °C. Under both conditions, the yield of W_6I_{18}, identified by crystal habit (rods) after the initial structure determination, was so low as to be undetected by X-ray powder diffraction. Previous reports have claimed the synthesis of materials approaching the composition WI_3 (Scheme 1). The products of two of these preparations[7,8] were apparently amorphous. A third report describes the synthesis of "silver needles" which analyzed as $WI_{3.0}$ from two different sealed tube preparations:[5] (1) reaction of tungsten metal and iodine in a 500–350 °C temperature gradient; (2) chemical transport of "$WI_{3.3}$" (W_4I_{13}?) in a 450–350 °C temperature gradient. The latter is consistent with our observation that sealed tube reactions of Phase B conducted in a *ca.* 350–400 °C range yield at the cooler end of the tube silver needles analyzing exactly as WI_3.[43] Unfortunately, the structure of this phase was not determined because the needles

Table 6. Selected Interatomic Distances (Å) and Angles (deg) for W_6I_{12}, W_6I_{16}, W_6I_{18}, and $[W_6I_8(CF_3SO_3)_6]^{2-}$

	W_6I_{12}	W_6I_{16}	W_6I_{18}	$[W_6I_8(CF_3SO_3)_6]^{2-}$
W–W	2.663–2.670	2.656–2.678	2.667–2.681	2.644–2.661
mean	2.665(3)	2.669(8)	2.674(4)	2.650(5)
W–μ_3-I	2.788–2.805	2.759–2.817	2.779–2.802	2.793–2.831
mean	2.795(6)	2.78(2)	2.791(7)	2.807(8)
W–I^a/O	2.797(5)	2.817(3)	2.828(2)	2.100–2.174
mean				2.14(3)
W–W–W^b	59.9–60.2	59.5–60.3	59.7–60.3	59.7–60.3
mean	60.0(1)	60.0(3)	60.0(1)	60.0(1)
W–W–W^c	89.7–90.3	89.7–90.3	89.7–90.3	89.7–90.2
mean	90.0(2)	90.0(2)	90.0(2)	90.0(2)
W–W–μ_3-I	61.3–61.9	60.4–62.3	61.0–61.9	61.5–62.5
mean	61.5(2)	61.4(5)	61.4(2)	61.8(2)
W–μ_3-I–W	56.8–57.2	56.3–57.7	57.0–57.5	56.0–56.7
mean	57.0(1)	57.3(4)	57.2(1)	5.63(2)
μ_3-I–W–μ_3-I	89.2–90.5	88.7–92.1	89.3–90.8	89.2–91.0
mean	89.9(4)	90(1)	90.0(4)	89.9(5)
μ_3-I–W–I^a/O	88.2–88.3	85.2–91.1	87.9–89.3	83.8–91.7
mean	88.3(1)	88(2)	88.5(5)	88(2)
μ_3-I–W–I^d	85.3–90.9	84.2–93.6	84.8–92.2	
mean	88(3)	88(3)	88(2)	

^{a} Terminally ligated (nonbridging) iodide atom. ^{b} Within triangular faces. ^{c} Within equatorial squares. ^{d} Bridging iodide or triiodide atom.

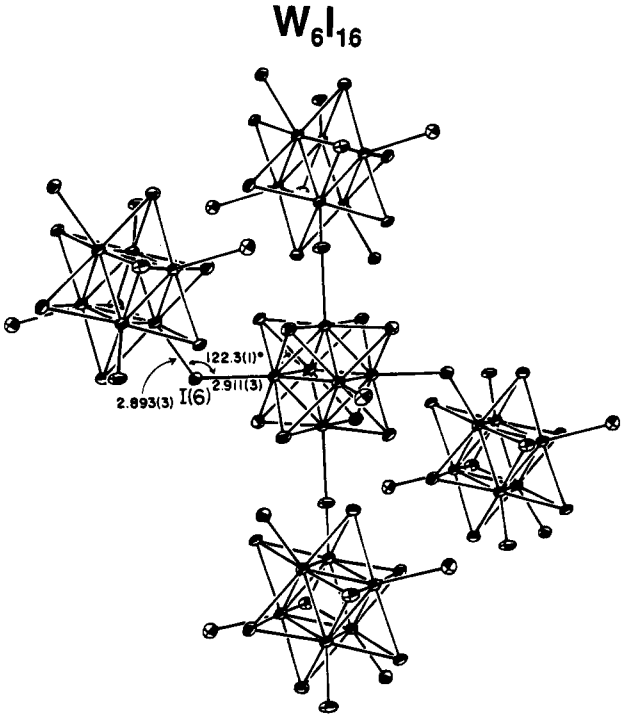

Figure 10. The structure of the two-dimensional phase $W_6I_{16} = [W_6I^i_8]$-$I^a_2I^{a-a}{}_{4/2}{}^{a-a}{}_{4/2}{}\cdot 2I_2$, showing iodide bridges between clusters and the bridge angle and distances; the iodine atoms are omitted. Each cluster resides on an inversion center; atoms are depicted as 70% probability ellipsoids.

were too thin for single-crystal X-ray diffraction work. X-ray powder diffraction data matched that previously reported for WI_3 and exhibited intense low-angle peaks characteristic of a cluster-containing phase (hence W_nI_{3n}). This material proved to be insoluble in any common solvent.

The structure of W_6I_{18} is presented in Figure 11; metric data are summarized in Table 6. Each $[W_6I_8]^{4+}$ core is linked to two neighbors via two nearly linear triiodides (I–I–I = 173.8-(2)°) and two iodide atoms (W–I–W = 134.0(1)°), affording the connectivity $[W_6I^i_8]I^a_2I^{a-a}{}_{2/2}(I_3)^{a-a}{}_{2/2}\cdot 2I_2$. Both the triiodide and the iodide bridges and *trans*, generating a one-dimensional structure. Two additional iodine molecules per cluster are present in the lattice. While W–W bond distances (mean 2.674-(4) Å) are not different from those in the preceding phases, mean values W–(μ_3-I) (2.791(7) Å) and terminal W–I (2.828(2) Å) bond lengths are somewhat longer. The origin of these lengthened distances is unclear. Other examples of M_6X_{18} phases include $W_6Cl_{18} = [W_6Cl^i_{12}]Cl^a_6$,[31] with a core containing 12 edge-bridging chloride atoms, and $W_6Br_{18} = [W_6Br^i_8]$-$Br^a_2(Br_4)^{a-a}{}_{4/2}$,[15] another example of clusters linked by Br_4^{2-}.

(d) $[W_6I_{14}]^{2-}$. In past accounts, the preparation of soluble $[W_6I_8]^{4+}$ core-containing species has generally proceeded via excision from W_6I_{12} with ethanol/HI reaction mixtures, producing $[W_6I_{14}]^{2-}$ in solution. Although such methods readily excise the analogous phases Mo_6X_{12} (X = Cl, Br, I) and W_6X_{12} (X = Cl, Br),[11] the technique has proven significantly less effective when applied to W_6I_{12}. In agreement with prior observations,[6] we find W_6I_{12} to be only sparingly soluble in ethanol/HI, leading to disappointingly low yields of $[W_6I_{14}]^{2-}$. Indeed, none of the previously reported syntheses of $[W_6I_{14}]^{2-}$ quantify a yield for this product. A much improved route to this cluster is attained by applying dimensional reduction[44] to W_6I_{12}. In accordance with this formalism, incorporation of KI breaks up the two-dimensional framework of W_6I_{12} producing a molecular solid of probable formula $K_2W_6I_{14}$ (analogous to $K_2Mo_6Cl_{14}$[45]), which completely dissolves in ethanol to give the desired species $[W_6I_{14}]^{2-}$ in solution. In the present work, this was accomplished by heating Phase B and KI under conditions which in the absence of KI afford W_6I_{12}.

When an intimate mixture of Phase B and KI is heated at 550 °C for 65 h, an orange-black solid is formed (presumably $K_2W_6I_{14}$) which contains the $[W_6I_{14}]^{2-}$ cluster anion. Dissolution of the solid in ethanol followed by addition of solid $(Bu_4N)I$ gave $(Bu_4N)_2[W_6I_{14}]$ in 30% yield (based on $W(CO)_6$). The compound was identified by FAB-MS and unit cell parameters.[12]

Cluster Buildup. The degree of reaction between tungsten metal and iodine appears to depend rather critically on the size of the metal particles. Direct reaction in a sealed tube at temperatures up to 800 °C leaves the elemental reactants largely unperturbed, producing an occasional crystal of W_6I_{12}, W_6I_{16}, or W_6I_{18}. Typically, a mixture of crystals from these three phases is observed in unpredictable proportions and negligible

(43) Anal. Calcd for WI_3: W, 32.57; I, 67.43. Found: W, 32.34; I, 67.51.

(44) Long, J. R.; Williamson, A. S.; Holm, R. H. *Angew. Chem., Int. Ed. Engl.* **1995**, *34*, 226.

(45) Potel, M.; Perrin, C.; Perrin, A.; Sergent, M. *Mater. Res. Bull.* **1986**, *21*, 1239.

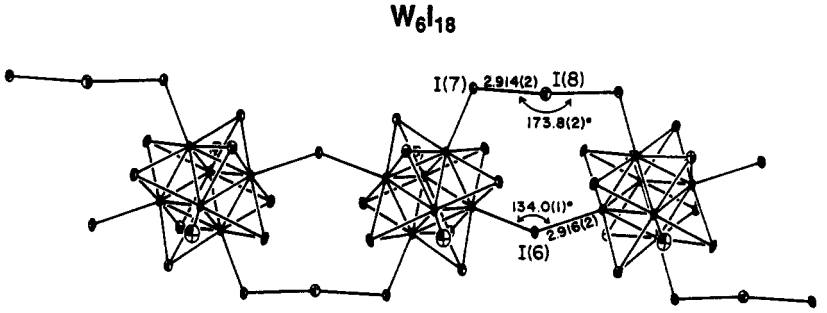

Figure 11. The structure of the one-dimensional phase $W_6I_{18} = [W_6I^i_8]I^a_2I^a_{2/2}(I_3)^{a-a}{}_{2/2}{\cdot}2I_2$ showing iodide and triiodide bridges between clusters, selected bridge bond angles and distances, and the bridge atom labeling scheme; the iodine molecules are omitted. Each cluster resides on an inversion center; atoms are depicted as 70% probability ellipsoids.

overall yields. The situation is somewhat improved when submicron particles of tungsten metal are used; however, the yields are only a few percent. The sluggishness of these reactions is surmounted by employing $W(CO)_6$ as the tungsten source. Upon heating, the compound is decarbonylated, generating open coordination sites on the zero-valent tungsten atoms, which readily react with the excess iodine to produce the many binary phases described herein (Scheme 2). As a reactant with iodine, $W(CO)_6$ was introduced as early as 1966,[8] but other than W_6I_{12}, no phase obtained from such reaction systems was structurally identified prior to this work (Scheme 1).

The nuclearity of clusters obtained increases as a function of temperature. This observation, coupled with the close structural relation between clusters, leads us to speculate that the encountered products might indicate the nucleation pathway for the formation of $[W_6I_{14}]^{2-}$. The proposed pathway is set out in Figure 12 and is described in terms of a sequence of formalistic transformations. The first stable aggregate isolated is triangular $[W_3I_9]^{1-}$, demonstrating that at temperatures as low as 140 °C, nucleation is already well underway. When the temperature is raised slightly to *ca.* 165 °C, one core W–I bond breaks, allowing $[W_3I_9]^{1-}$ to open up, exposing a triangular face which is capped by a WI_2 unit (I–W–I *ca.* 90°) to form tetrahedral $[W_4I_{11}]^{1-}$ (as found in W_4I_{13}). In total, this first transformation involves breaking one W–I bond and forming three new W–W and four new W–I bonds. At slightly higher temperatures (200–300 °C), a nearly identical process takes place, in which one core W–I bond and the long W–W bond breaks, opening $[W_4I_{11}]^{1-}$ into a butterfly geometry that accommodates another WI_2 unit to form square-pyramidal $[W_5I_{13}]^{1-}$ (as in W_5I_{16}). As before, three W–W and four W–I bonds are formed in the transformation. Finally, at *ca.* 550 °C, without rearrangement, $[W_5I_{13}]^{1-}$ accepts a $[WI]^{1-}$ unit which caps its square face to produce the octahedral $[W_6I_{14}]^{2-}$ cluster (as in W_6I_{12} and W_6I_{16}). This last transformation involves the formation of four W–W and four W–I bonds.

The four binary clusters observed in the reaction between $W(CO)_6$ and iodine ($[W_3I_9]^{1-}$, $[W_4I_{11}]^{1-}$, $[W_5I_{13}]^{1-}$, and $[W_6I_{14}]^{2-}$) constitute a distinct set of polyhedra-based structures. Two simple structural principles appear to govern this family of tungsten–iodine clusters. First, all of their structures are composed of *WI_5 square pyramids sharing basal edges*. Second, all of the clusters are *uniterminally ligated*,[46] in that the axially-coordinated I atoms are the only tungsten ligands which are terminal rather than bridging. Structures fulfilling the first criteria are generated by wrapping fragments of a fictitious, two-dimensional parent solid $SPy_2(1_4)SPy_1(1_4)-{}^2_\infty WI_2$, whose structure may be assembled by close packing WI_5 square pyramids on a flat surface such that their basal iodine atoms form a regular square lattice.[47] Applying our second criterion (uniterminal ligation) to the structures so derived extricates a comprehensive collection of clusters with the desired structural properties. The smallest structure (and the only trinuclear structure) in this collection corresponds to the smallest binary

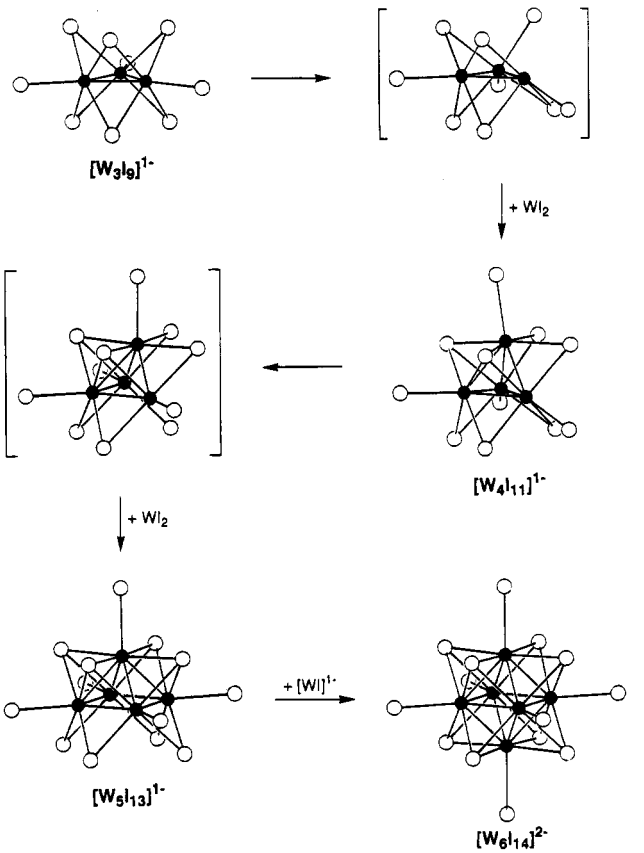

Figure 12. Proposed nucleation pathway for tungsten–iodide clusters terminating with the formation of $[W_6I_{14}]^{2-}$. Breaking one W–μ_2-I bond in triangular $[W_3I_9]^{1-}$ generates a slightly rearranged intermediate species (first set of brackets) which readily accommodates a WI_2 moiety (I–W–I angle *ca.* 90°) to form the tetrahedral $[W_4I_{11}]^{1-}$ unit of W_4I_{13}. Breaking two bonds (the long W–W bond and an associated W–μ_2-I bond) in this tetrahedral cluster allows it to expand into an intermediate cluster fragment with a butterfly geometry (second set of brackets). Subsequent or simultaneous incorporation of a WI_2 unit (I–W–I angle *ca.* 90°) yields the square-pyramidal $[W_5I_{13}]^{1-}$ cluster, and, finally, insertion of a $[WI]^{1-}$ moiety produces the octahedral $[W_6I_{14}]^{2-}$ cluster. As shown, this sequence serves to emphasize the close structural relationships between the four observed cluster motifs.

(46) You, J.-F.; Holm, R. H. *Inorg. Chem.* **1992**, *31*, 2166.

(47) The Polyhedra Connectivity Partitioning (PCP) notation and sheet wrapping procedure employed here, as well as other aspects of deriving cluster structures from parent solids, are described in: Long, J. R.; Holm, R. H. *J. Am. Chem. Soc.* **1994**, *116*, 9987.

tungsten–iodine cluster observed, $SPy_2(3_2)$–$[W_3I_9]^{1-}$ (Figure 2). It represents the first member in a series of cyclic clusters $SPy_2(m_2)$–$[W_mI_{3m}]^{z-}$ (m = 3, 4, 5, ...) wherein m WI_5 square pyramids share *trans* basal edges. The second (m = 4) member in the series, $SPy_2(4_2)$–$[W_4I_{12}]^{z-}$, has the same structure as the square isomer of $[Mo_4Cl_{12}]^{3-}$, shown on the left in Figure 1.[21] There is no evidence suggesting the existence of such a species during the nucleation of $[W_6I_{14}]^{2-}$, nor is its structure consistent with the proposed pathway (Figure 12); however, on a purely structural basis, square $[W_4I_{12}]^{z-}$ does present a valid synthetic target. The stability of higher nuclearity (m > 4) cyclic clusters is somewhat less likely, because as m increases the W atoms are forced further apart, weakening the W–W bonding interactions apparently required to support low-valent tungsten iodides. The other isomer of $[Mo_4Cl_{12}]^{3-}$ (shown on the right in Figure 1)[21] is not uniterminally ligated; however, when this structure is folded such that the two terminal basal iodine atoms fuse (*i.e.*, such that the two square-pyramid bases now share a corner), the tetrahedral geometry of $SPy_2(2_32_2)SPy_1(2_1)$–$[W_4I_{11}]^{1-}$ (Figure 3) is obtained. Here, uniterminal ligation is achieved at the expense of rigorous square-pyramidal stereochemistry at the tungsten centers, which must be slightly distorted to make the fold (see Table 4). Wrapping a cube with penta- and hexanuclear fragments of the WI_2 parent solid produces the uniterminally ligated structures of square-pyramidal $SPy_2(1_44_3)$–$[W_5I_{13}]^{1-,2-}$ (Figure 4) and octahedral $SPy_2(6_4)$–$[W_6I_{14}]^{2-}$ (Figure 12, bottom right), respectively. Although larger polyhedra containing edge-sharing square faces may also be wrapped with WI_2 fragments (for example, a rhombicuboctahedron[48] may be wrapped to produce $SPy_2(6_412_2)SPy_1(12_4)$–$[W_{18}I_{42}]^{z-}$), the resulting structures are likely to be unstable, since, as with the large cyclic clusters, they necessarily contain well-separated tungsten atoms. Thus, the $[W_6I_{14}]^{2-}$ structure completes the tungsten–iodine cluster family, just as it provides a terminus in the solid-state reaction between $W(CO)_6$ and iodine.

Terminal Ligand Substitution. In general, the clusters $[M_6X_{14}]^{2-}$ (M = Mo, W) sustain core halide substitution reactions under forcing conditions[6,49] but exhibit relatively facile terminal ligand substitution reactions. Numerous clusters of the types $[M_6X_8Y_6]^{2-}$ and $[M_6X_8Y_4L_2]$, where Y is a halide, pseudohalide, hydroxide, methoxide, or triflate and L is a neutral ligand, have been prepared by substitution or by the related process of cluster excision.[6,11,13,49a,d,e,50,51] We have chosen to replace iodide with triflate in order to obtain clusters of high substitutional lability for use in subsequent work. Following the procedure of Shriver and co-workers[51] for $[Mo_6Cl_8(CF_3SO_3)_6]^{2-}$, $(Pr_4N)_2[W_5I_8(CF_3SO_3)_5]$ was obtained in 51% yield by the reaction of $(Pr_4N)_2[W_5I_{13}]$ and excess $Ag(CF_3SO_3)$ in dichloromethane. In an analogous reaction, $(Bu_4N)_2[W_6I_8(CF_3SO_3)_6]$ was isolated in 81% yield.[52] The structures shown in

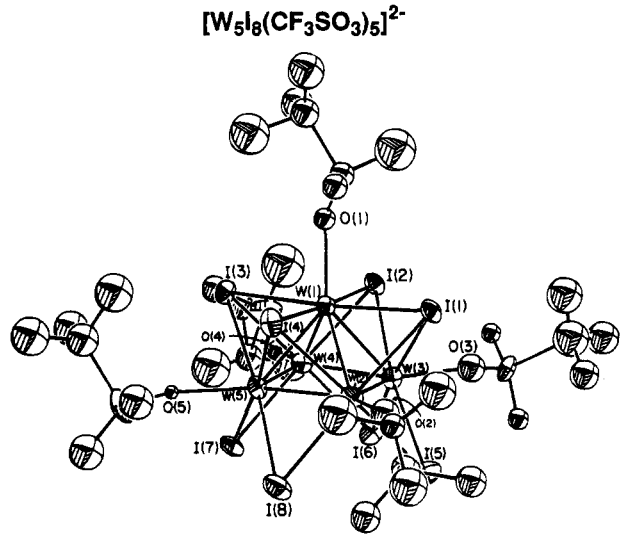

Figure 13. The structure of $[W_5I_8(CF_3SO_3)_5]^{2-}$ as the $(Pr_4N)^+$ salt, showing the atom labeling scheme and 50% probability ellipsoids.

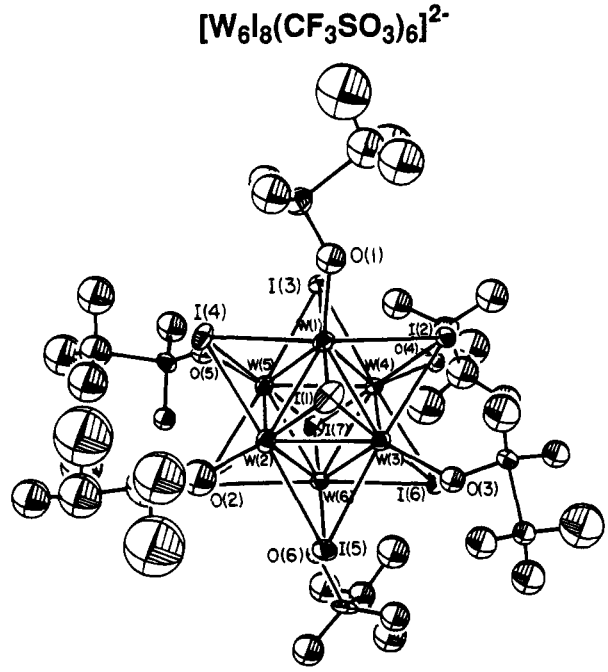

Figure 14. Structure of $[W_6I_8(CF_3SO_3)_6]^{2-}$ as the $(Ph_4P)^+$ salt, CH_2Cl_2 adduct; shown are the atom labeling scheme and 30% probability ellipsoids.

Figures 13 and 14 and the metric data in Tables 4 and 5 substantiate the desirable properties of terminal ligand substitution with core retention. Interestingly, although the core dimensions in both clusters are largely preserved upon substitution, the pentanuclear cluster undergoes a rhombic distortion in the base of its W_5 square pyramid (W(2)–W(3)–W(4) = 95.1(2)°, W(3)–W(4)–W(5) = 84.9(2)°, W(4)–W(5)–W(2) = 95.1(1)°, and W(5)–W(2)–W(3) = 84.6(2)°). The mean W–O distances of 2.15(4) Å in $[W_5I_8(CF_3SO_3)_5]^{2-}$ and 2.14(3) Å in $[W_6I_8(CF_3SO_3)_6]^{2-}$ are roughly comparable with that in $[Mo_6Cl_8(CF_3SO_3)_6]^{2-}$ (2.126(9) Å),[51] but the esd's of individual bond lengths are rather large. Preliminary observations indicate the high lability of the triflate ligands in substitution reactions with a variety of other ligands.

Summary

The reaction between $W(CO)_6$ and iodine has been exploited in monitoring the solid-state nucleation of $[W_6I_{14}]^{2-}$, while

(48) Wenninger, M. J. *Polyhedron Models*; Cambridge University Press: Cambridge, England, 1971; p 27.

(49) (a) Sheldon, J. C. *J. Chem. Soc.* **1962**, 410. (b) Baumann, H.; Plautz, H.; Shäfer, H. *J. Less-Common Met.* **1971**, *24*, 301. (c) Sheldon, J. C. *Chem. Ind. (London)* **1961**, 323. (d) Nannelli, P.; Block, B. P. *Inorg. Chem.* **1966**, *7*, 2423. (e) Chisholm, M. H.; Heppert, J. A.; Huffman, J. C. *Polyhedron* **1984**, *3*, 475. (f) Michel, J. B.; McCarley, R. E. *Inorg. Chem.* **1982**, *21*, 1864. (g) Ebihara, M.; Toriumi, K.; Saito, K. *Inorg. Chem.* **1988**, *27*, 13. (h) Hilsenbeck, S. J.; Young, V. G., Jr.; McCarley, R. E. *Inorg. Chem.* **1994**, *33*, 1822.

(50) (a) Cotton, F. A.; Curtis, N. F. *Inorg. Chem.* **1965**, *4*, 241. (b) Saito, T.; Nishida, M.; Yamagata, T.; Yamagata, Y. *Inorg. Chem.* **1986**, *25*, 1111. (c) Saito, T.; Manabe, H.; Yamagata, T.; Imoto, H. *Inorg. Chem.* **1987**, *26*, 1362.

(51) Johnston, D. H.; Gaswick, D. C.; Lonergan, M. C.; Stern, C. L.; Shriver, D. F. *Inorg. Chem.* **1992**, *31*, 1869.

(52) This compound was first prepared in the laboratories of Nycomed Salutar, Inc. (Droege, M. W., private communication).

simultaneously producing a host of phases containing binary tungsten–iodine clusters (Scheme 2). The following are the principal results and conclusions from this investigation.

(1) The reaction commences with the liberation of CO gas, facilitating nucleation which, when halted at 140 °C, has already proceeded to the formation of an amorphous black solid (Phase A) containing trinuclear $[W_3I_9]^{1-}$ clusters. This species is isolated from solution as its $(Bu_4N)^+$ salt and exhibits a new structure type (Figure 2), consisting of a W_3 triangle surrounded by six edge-bridging (two per edge) and three terminal iodides.

(2) Heating Phase A in a sealed tube at 165 °C affords an insoluble black, crystalline phase, W_4I_{13}. The structure of this molecular compound features tetrahedral $[W_4I_{11}]^{1-}$ clusters dimerized via two bridging triiodide units (Figure 3).

(3) Further heating at 200 °C propels nucleation to the pentanuclear stage with the formation of an amorphous solid (Phase B) containing $[W_5I_{13}]^{1-}$ clusters. This contention is supported by the emergence, upon continued heating at 250 °C, of crystalline W_5I_{16}, an extended solid possessing one-dimensional chains of $[W_5I_{13}]^{1-}$ clusters linked by triiodide units (Figure 4). Phase B readily dissolves in ethanol, enabling the isolation of $[W_5I_{13}]^{1-}$ as its $(Pr_4N)^+$ salt; the structure of the latter reveals square-pyramidal clusters (Figure 5, upper) bearing an obvious similarity to the octahedral geometry of $[W_6I_{14}]^{2-}$.

(4) Reduction of $[W_5I_{13}]^{1-}$ with Zn in a dichloromethane solution yields $[W_5I_{13}]^{2-}$ which retains its square-pyramidal structure (Figure 5, lower) with only very minor metric differences (Table 5). Reaction of the dianion with $Ag(CF_3SO_3)$ in dichloromethane replaces the terminal iodides with substitutionally labile triflate ligands to form $[W_5I_8(CF_3SO_3)_5]^{2-}$ (Figure 13).

(5) Heating Phase A with CsI at 300 °C produces, among other phases, crystalline CsW_5CI_{16}, containing $[W_5(C)I_{13}]^{1-}$ clusters which interact with Cs^+ as shown in Figure 7. This pentanuclear carbide cluster is isolated in pure form as its $(Bu_4N)^+$ salt by means of solubility and displays a novel structure (Figure 8) in which the square base of $[W_5I_{13}]^{1-}$ is capped with a carbon atom. The source of the carbon atom is most likely residual CO in Phase A.

(6) Heating Phase B at 550 °C under a variety of conditions (see Scheme 2) affords a number of solid phases, including W_6I_{12} (Figure 9) and W_6I_{16} (Figure 10), composed of octahedral $[W_6I_{14}]^{2-}$ cluster units. This cluster represents the endpoint in the nucleation process and is produced in molecular form at high yield (30% based on $W(CO)_6$) by solubilizing its K^+ salt. Entry into the ligand substitution chemistry of the $[W_6I_8]^{4+}$ core is accessible via $[W_6I_8(CF_3SO_3)_6]^{2-}$ (Figure 14) which is prepared in a manner analogous to that of its pentanuclear analogue.

(7) Results 1–3 and 6 above establish the following sequence of intermediate species in the solid-state nucleation of $[W_6I_{14}]^{2-}$: $[W_3I_9]^{1-} \rightarrow [W_4I_{11}]^{1-} \rightarrow [W_5I_{13}]^{1-} \rightarrow [W_6I_{14}]^{2-}$. The structural relationships between intermediates are consistent with a specific nucleation pathway (Figure 12), providing a degree of detail not previously exposed for cluster nucleation in the solid state.

Acknowledgment. This research was funded by a grant from Nycomed Salutar, Inc. and Grant No. CHE 92-0387 from the National Science Foundation. We thank the Office of Naval Research for their support of J.R.L. in the form of a predoctoral fellowship (1991–94), Drs. M. W. Droege and A. D. Watson for useful discussions, and B. Souza for technical assistance.

Supporting Information Available: X-ray structural information for the compounds in Tables 1 and 2, including tables of crystal and intensity collection data, positional and thermal parameters, and interatomic distances and angles (72 pages). This material is contained in many libraries on microfiche, immediately follows this article in the microfilm version of the journal, can be ordered from the ACS, and can be downloaded from the Internet; see any current masthead page for ordering information and Internet access instructions.

JA951265U